UNIVERSITY OF OKLAHOMA

GRADUATE COLLEGE

USING RADIOSONDE OBSERVATIONS TO ASSESS THE 'THREE-INGREDIENTS' METHOD TO FORECAST QLCS MESOVORTICES

A THESIS

SUBMITTED TO THE GRADUATE FACULTY

In partial fulfillment of the requirements for the

Degree of

MASTER OF SCIENCE IN METEOROLOGY

By

MAX DAVID UNGAR
Norman, Oklahoma
2022

USING RADIOSONDE OBSERVATIONS TO ASSESS THE 'THREE-

INGREDIENTS' METHOD TO FORECAST QLCS MESOVORTICES

A THESIS APPROVED FOR THE

SCHOOL OF METEOROLOGY

BY THE COMMITTEE CONSISTING OF

Dr. Michael Coniglio, Chair

Dr. Michael Biggerstaff

Dr. James Ruppert

# Acknowledgements

This thesis could not have been completed without the help and encouragement of many the past few years. First and foremost, to my family, thank you for always helping to foster my passion for weather/severe weather. I appreciate you always "listening" to me talk about a random severe weather event thousands of miles away most evenings in the spring and summer. Your encouragement and advice while I've been at OU have allowed me to maximize my time here, and for that, I'm forever grateful.

I want to thank my advisor, Dr. Mike Coniglio, for his support on this project. This work was completed in nearly a full virtual setting due to the COVID-19 pandemic. Despite these challenges, Mike was always there to offer his advice or help in any way to help make this research fruitful. I also want to thank my committee members, Drs. Mike Biggerstaff and James Ruppert, for their roles in helping improve this manuscript and project conclusions. This work also greatly benefited from conversations with Jason Schaumann, Science and Operations Officer at the National Weather Service in Springfield, MO. His insights on this work were invaluable in helping refine research areas/topics, especially concerning development of the mesovortex analysis criteria.

I'm thankful for the National Weather Center community for always providing inspiration to be the best scientist every day. Beyond the research campus, I'm very thankful for the support my friends have provided the last few years. Whether it was playing intramural sports together, or enjoying a game of bingo at BIG, these moments always provided me joy. Finally, I especially want to thank Lauren Pounds for her endless support and encouragement while I've worked on this project.

Boomer Sooner!

# Table of Contents

# List of Figures

# Abstract

Quasi-linear convective system (QLCS) mesovortices have a propensity to produce impactful severe weather outcomes, including tornadoes and enhanced straight-line wind damage. Despite advances in understanding the origins of these meso-gamma scale vortices over the past two decades, a relative lack of operational tools remain for anticipating their genesis. In particular, genesis of these features can occur over small temporal scales, presenting a challenge in current warning operations.

One tool used widely in the forecasting community is the "Three Ingredients" Method (3-I-M), developed by Schaumann and Przybylinski (2012), which identifies favored QLCS mesovortexgenesis conditions for operational benefit. The 3-I-M assesses both internal system characteristics along with the pre-convective environment to aid in early identification of mesovortex potential. The 3-I-M are 1) a portion of a QLCS in which the system cold pool and ambient low-level shear are said to be nearly "balanced" or "slightly shear dominant", 2) where 0-3 kilometer line-normal bulk wind shear magnitudes are greater than or equal to 15 m s$^{-1}$, and 3) where a rear-inflow jet or enhanced outflow causes a surge or bow along the convective line. Despite its widespread use as a tool to predict QLCS mesovortices, this method has not been evaluated extensively in formal literature.

To evaluate the 3-I-M using data not available for the Schaumann and Przybylinski (2012) founding study, environmental data from radiosonde observations in proximity to 50 observed QLCSs, including 9 from past field programs (PECAN, VORTEX-SE, MESO18-19), were compared against QLCS characteristics revealed by nearby WSR-88D observations. Analysis of internal characteristics included assessing the shear/cold pool balance, rear-inflow surges, and observed mesovortices. Analysis shows that nearly half (46%) of mesovortexgenesis

events were observed in regimes of sub-critical line-normal 0-3 km wind shear. This agrees with recent studies that found mesovortexgenesis processes can be quite varied and can occur for line-normal shear under the 15 m s$^{-1}$ threshold. Additionally, the distance between the Updraft Downdraft Convergence Zone (UDCZ) and elevated reflectivity, related to shear/cold pool balance, appears to offer more skill in discriminating mesovortexgenesis potential than line-normal 0-3 km wind shear. This study also offers potential objective criteria for defining favorable shear/cold pool balance "regimes", along with magnitudes of wind shear across both deeper and shallower depths, favorable for mesovortexgenesis.

# Chapter 1: Introduction and Background

## 1.1. QLCS Mesovortex Hazards and Genesis Mechanisms

Quasi-linear convective systems (QLCSs), linear assemblages of convection, can pose a significant risk to both life and property. In particular, the generation of QLCS mesovortices (MVs) increase the propensity of these systems to produce both damaging straight-line winds and tornadoes. Numerous observational studies have shown these features are capable of producing both tornadoes and swaths of straight-line wind damage (Atkins et al. 2005; Wakimoto et al. 2006b; Wheatley et al. 2006). In fact, approximately 20% of tornadoes across the central and eastern United States are attributable to QLCS storm morphologies (Trapp et al. 2005; Haberlie et al. 2019). While a large proportion of QLCS mesovortex tornadoes are weak, (E)F-0 or (E)F-1, strong/intense QLCS tornadoes do occur (Trapp et al. 2005; Smith et al. 2012). Beyond the presence of severe convective hazards, mesovortices can develop in short temporal scales, presenting a challenge in current warning decision making. Brotzge et al. (2013) and Gibbs and Bowers (2019) note that QLCS tornadoes have a lower probability of detection (POD) and a higher number of "missed events" for significant (EF2+) tornadoes than their supercell counterparts.

Understanding the mechanisms behind the generation of MVs in linear systems has greatly advanced in the past two decades. A leading theory for mesovortexgenesis (henceforth mv-genesis) is the tilting and stretching of baroclinic horizontal vorticity, generated by the cold pool, by either 1.) updrafts or 2.) convectively-induced downdrafts (Trapp and Weisman 2003, Atkins and St. Laurent 2009a,b). Mechanisms other than those related to the tilting of baroclinic horizontal vorticity are known to contribute to mv-genesis including the release of horizontal shear instability (HSI) (Carbone 1983; Lee and Wilhelmson 1997a,b; Wheatley and Trapp 2008;

Conrad and Knupp 2019) and tilting/stretching of frictionally-induced vorticity (Schenkman et al. 2012) . Recent studies note that mv-genesis mechanisms may be quite varied including processes similar to those of mesocyclones in supercells, including downward tilting of horizontal vorticity associated with descending rear-inflow and ingestion of low-level streamwise vorticity, or from combinations of all above processes discussed above (Xu et al. 2015a,b; Flournoy and Coniglio 2019).

## 1.2. The 'Three-Ingredients' Method For Forecasting MVs

Despite growing knowledge of plausible mv-genesis mechanisms, a relative lack of predictive tools currently exist in operational settings to assist forecasters in identifying mv-genesis signals using conventional single or dual-polarization products. The "Three Ingredients" method (henceforth 3-I-M), developed by Schaumann and Przybylinski (2012) (henceforth SP12), identifies favored QLCS mv-genesis conditions to help in their early prediction and warning.

*The first ingredient of the 3-I-M framework describes the relationship between ambient environmental shear and the system cold pool, which is favorable when it is nearly "balanced" or "slightly shear dominant".* Physically, this ingredient attributes a vertically-oriented updraft along the cold pool to a relative "balance" between horizontal vorticity rotors generated by 1) baroclinic vorticity at the edge of the cold pool/gust front and 2) from the ambient environmental wind shear (Rotunno et al. 1988, Weisman and Rotunno 2004). In a "balanced" regime, updrafts tend to be vertically upright and deep, with a maximum in constructive interference between the environmental shear and cold pool. The theoretical simulations of Atkins and St. Laurent (2009a,b) identified that deep/upright updrafts at the gust front edge also facilitates efficient stretching of near-surface vertical vorticity. Updrafts within "slightly shear dominant" modes are

2

forward leaning and slightly weaker than their "balanced" counterparts. The horizontal vorticity rotor tends to pull parcels downshear from (and atop) the cold pool interface. An overview of idealized simulations showing these different shear/cold balance regimes, conducted by Weisman and Pryzbylinski (1999), is shown as Figure 1. This 'balance', between the cold pool circulation and opposing low-level shear, is difficult to quantify in observations because knowledge of cold pool depth is required. Therefore, it is often estimated via radar imagery by assessing the distance between convection and the leading edge of the cold pool. Small distances are assumed to represent a cold pool balanced by line-normal low-level shear over the lowest few kilometers.

*The second ingredient of the 3-I-M is achieved when the magnitude of the environmental wind shear in the lowest 3 km above ground level (AGL) normal to the convective system meets or exceeds 15 m s$^{-1}$ (30 kt).* The idealized experiments of Trapp and Weisman (2003) identified 20 m s$^{-1}$ of (unidirectional) wind shear in the 0-2.5 km layer to favor the presence of cyclonic surface vortices within QLCSs. Concurrently, Atkins and St. Laurent (2009a) note that, using varied magnitudes of wind shear in the 0-2.5 km and 0-5 km AGL depths, weaker and shorter-lived MVs tend to develop in regimes of wind shear magnitudes < 15 m s$^{-1}$ (although cold pool strengths in these studies were not varied).

SP12 note that the physical significance of the 15 m s$^{-1}$/30 kt threshold is unclear, though it is assumed that it is tied to the shear/cold pool vorticity balance principles described in Rotunno et al. (1988) and Weisman and Rotunno (2004). Weaker low-level shear tends to promote a cold pool circulation that "overwhelms" the opposing ambient vorticity. Highlighting the work of Engerer et al. (2008), which calculated cold pool pressure rises within 39 mesoscale convective systems (MCSs) across Oklahoma, an approximation of environmental wind shear

3

required to promote "balance" across the depth a theoretical cold pool was 14-16 m s$^{-1}$. Orientation of wind shear vectors also plays a critical role in determining the nature of lifting potential at the cold pool/gust front interface. SP12 note that the potential for updraft growth in this region is enhanced when vorticity rotors are "converging" (i.e. rotating in an upward direction). Therefore, it is thought that assessing the component of environmental wind shear orthogonal to the convective line (i.e. "line-normal") is crucial in understanding wind shear control for promoting differing shear/cold pool balance regimes.

The concepts discussed above tend to ignore the impact of deeper-layer shear for helping maintain convention near the leading edge of cold pools (Coniglio et al. 2006), as well as other potential physical explanations for why *some* low-level shear seems necessary in "balanced" regimes. This includes the impact of low-level shear on increasing storm-relative flow and reducing entrainment in leading convection, particularly under more "slabular" lifting (Alfaro 2017; Mulholland et al. 2021), or the balance of momentum between the cold pool and inflowing air (Bryan and Rotunno 2014; Alfaro and Lenaza 2022). Regardless of the underlying physical mechanism, the rationale for the 15 m s$^{-1}$ threshold is that some low-level shear is needed to promote organized linear convection along with a cold pool that remains tethered to nearby deep convection, a prerequisite for mv-genesis.

*The third ingredient discussed within the 3-I-M framework is the presence of a surge or bow within the main convective line, caused by a rear-inflow jet (RIJ) or enhanced outflow.* The RIJ feature associated with linear convective complexes has been extensively studied since the mid-twentieth century, with Fujita (1978) describing the damage potential of the descending RIJ at the convective system apex. Additional studies (Jorgensen and Smull 1993; Pryzbylinski 1995; Atkins et al. 2004) have further validated early findings and have shown that surface wind

damage can often be traced to the presence of a mesoscale RIJ. The physical importance of a RIJ surge to mv-genesis isn't entirely known, but one direct possibility is the cyclonic shear vorticity on the north side of the surge can be stretched into mv strength. Recent work of Xue et al. (2015) and Flournoy and Coniglio (2019) have identified a mv-genesis mechanism related to the downward tilting and stretching of streamwise vorticity stemming from the descending behavior of smaller-scale RIJs embedded within QLCSs. Atkins et al. (2004) also noted that all tornadic vortices observed within a QLCS during the BAMEX field campaign formed coincident with the genesis of an RIJ.

To explore environmental controls on QLCS mv-genesis (and tornadic) potential, this study assesses both internal QLCS characteristics and potential environmental forcings in relation to 50 observed QLCSs across the CONUS. Internal system characteristics are evaluated using WSR-88D observations. Such observations are used to assess relative shear/cold pool balance of each system (ingredient #1), RIJ features (ingredient #3), and observed mesovortex outcomes. Radiosonde observations from both field program and operational (National Weather Service) settings will help explore the impact of varying shear magnitudes, across varying depths, for mv-genesis outcomes.

The primary goals of this study are to evaluate the 3-I-M, identify scenarios where the 3-I-M may not properly identify QLCS mv-genesis, and to develop operational recommendations for operational settings in these scenarios. To the authors knowledge, this study represents one of the few to quantitatively test the 3-I-M approach over a large dataset of observed cases. Of particular note, Gibbs (2021) assessed the 3-I-M, along with combinations of environmental mv-genesis precursors outlined by National Weather Service (NWS) Warning Decision Training Division (WDTD) guidance, to assess its skill in identifying mv-genesis tornado environments.

The 3-I-M was found to demonstrate reasonable skill for QLCS tornado prediction, especially when combined with additional environmental variables ("confidence builders" and "nudgers" in WDTD guidance). The discussion herein differs from Gibbs (2021) in a few fundamental ways. First, this study attempts to objectively quantify the shear/cold pool balance regime observed with each study QLCS by computing distance between updrafts and leading edge of the cold pool. Additionally, the assessment of environmental wind shear sensitivity from proximity soundings is a novel approach of this discussion.

Chapter 2 will discuss the data and analysis methods applied to assess the 3-I-M ingredients. In Chapter 3, an overview of 3-I-M performance across the dataset of cases will be presented. Finally, a discussion of key outcomes and possible operational recommendations will be discussed in Chapter 4 and 5 respectively.

# Chapter 2: Data and Analysis Methods

## 2.1. Case Selection Overview

To quantitatively assess the performance of the 3-I-M, a large dataset of QLCS events, spanning the period 1 January 2010 through 31 December 2020, was constructed. This included evaluation of all intensive operating periods (IOPs) across multiple field experiments conducted in the 2010s. The field experiments evaluated were the Plains Elevated Convection At Night (PECAN) and Verification of the Origins of Rotation and Tornadoes EXperiment-Southeast (VORTEX-SE/MESO18-19) campaigns. In addition, all convective periods (1200 UTC-1200 UTC) spanning the above period within the Storm Prediction Center (SPC) Storm Events Database, that observed ≥ 1 severe wind or tornado report, were also included for preliminary analysis.

Given the 3-I-M relates to linear or quasi-linear convection, composite (column-maximum) radar reflectivity imagery was interrogated for every potential IOP or convective period of interest to determine primary storm mode. This was done using the Interactive (composite) Radar Map from the National Center for Environmental Data (NCEI) (Figure 2). While many objective (radar) quantifications of QLCSs exist in the literature, this study applies the definition of Haberlie and Ashley (2019) which defines a QLCS as a contiguous or semi-contiguous line of convective cores (≥ 40 dBZ) that persists at least three hours. Applying this criteria, over 500 potential dates were identified as containing a potential QLCS of use for this report.

Potential study dates were further refined to isolate QLCSs that could be coupled to a nearby field experiment or operational radiosonde (sounding) launch. Proximity soundings were also investigated for unrepresentative or erroneous observations in this step of case reduction as

well. Omitting cases that had minimal spatial/temporal proxy to an operational or field program sounding release, or issues with unrepresentative data (post-convective launch, superadiabatic lapse rates, web-bulb effect, etc.), refined the case dataset total to 244 QLCSs (22 field program/222 "operational") and 428 sounding launches.

Continued case winnowing was undertaken to focus on QLCSs with short spatiotemporal lag to the appropriate proximity sounding(s). An initial time criteria of $\leq 3$ hours and distance $\leq 200$ km was applied to the remaining 244 QLCSs. In other words, for a QLCS to pass this round of reduction, its leading convective line had to arrive at the launch location $\leq 3$ hours after the time the sounding was launched, or have any portion of its convective line $\leq 200$ kilometers at the time of release. The NECI Interactive Radar Map contains a distance estimator tool that allowed for the distance criteria to be assessed. After applying the $\leq 3$ hour/$\leq 200$ km threshold, the remaining 244 potential events were winnowed to a total of 125 QLCSs (18 field program/107 "operational") tied with 208 individual proximity soundings.

The remaining 125 QLCSs were further interrogated using Level-II radar data, accessed via NCEI/Amazon Cloud Database, using the Gibson Ridge 2 Analyst (GR2Analyst) version 2.80 software. The goal of continued case refinement was done to identify QLCSs that 1) best maintained the definition of Haberlie and Ashley (2019) while approaching the launch location and 2) had short spatiotemporal lag to the appropriate proximity sounding. Potvin et al. (2010) notes that the optimal sampling zone for proximity soundings lies between 0-2 hours before and at a distance of 40-80 km from the feature of interest. While the Potvin et al. (2010) study was controlled against a different hazard (significant tornado reports), this discussion utilized this criteria as a guide for final case selection/winnowing.

In total, 50 individual QLCSs (with single associated proximity sounding) were selected for final analysis in this report. Selected cases were chosen as those with shortest distance/time lag to sounding release location that also maintained the applied QLCS definition of this report. Figure 3 highlights a comparison distribution of selected cases to that of cases meeting the intermediate < 3 hour/200 km threshold. A mean QLCS distance of ~95 kilometers from launch site and time-to-arrival of ~75 minutes closely matches the criteria of Potvin et al. (2010) for optimal utilization of proximity soundings. This included ~80% of cases arriving ≤ 120 minutes (2 hours) and ~50% being located ≤ 80 km from the sounding launch location at the time of release.

Figure 4 displays an overview of the geographical distribution of all operational and mobile field program launch sites. While not a one-to-one representation, these locations serve as a proxy for regions where study QLCSs occurred/were assessed. As such, the regional dispersion of cases matches well with previous QLCS climatological studies (Haberlie and Ashley 2019, Smith et al. 2012). Most notably, with the highest density of QLCS events across the Mississippi, Ohio, and Missouri River basins. The climatological relationship extends to the seasonality of study events as well (Figure 5), with ~60% of study QLCSs occurring between the months of April-July.

## 2.2. Establishing Criteria for Radar Analysis

Prior to the radar analysis methods of this project (discussed in Sections 2.3-2.6), utilizing GR2Analyst, a few analytical criteria were established. The first being that radar analysis of internal QLCS characteristics did not extend beyond 100 km (approximately 50 nautical miles) in radius from the single-site radar of use for a given case. Physical justification for this approach centers around mesovortex radar analysis, and limitations in that process

(described in Section 2.6). An example of this criterion applied to a study event, along with the implications on portions of a QLCS available for radar interrogation, is shown in Figure 6.

The second condition applied to the radar analysis methodology was assessment of QLCS characteristics over the final hour prior to system arrival at the location of the proximity sounding launch. Physically, this was done to best assess the possible interaction between internal QLCS behavior (via WSR-88D observations) and environmental controls assessed via the proximity sounding. The time of QLCS "arrival" (henceforth T0) was assessed by determining the time of last full volume scan prior to convective cores overspreading the launch location. Once T0 was identified for a case, each full-volume scan sampled during the preceding hour was valid for further interrogation.

Locations of sounding launches for operational (NWS) soundings were often tied to the position of the single-site WSR-88D radar of use for analysis. For these operational QLCS events, where radar and sounding launch sites were co-located, T0 was identified (i.e. radar analysis ceased) when the first echoes of the convective line breached the radar "cone-of-silence". For all nine field program (along with a small subset of operational) events, the sounding launch location and radar site used in the analysis were not co-located. For these events, the 100 km (radial) maximum analysis distance, centered at the single-site radar of use, was maintained. However, T0 was now determined when the QLCS breached the sounding launch site. To help identify launch locations when determining T0 for "mismatched" cases, a small (~2 km) range ring was created using the Iowa Environmental Mesonet (IEM) ring creator tool, and viewed within the GR2Analyst software. An example of a "mismatched" case, from 9 October 2018 in central Oklahoma, is shown in Figure 7.

A final criteria applied for the radar methods was only conducting analysis at every other full volume scan within the previously described range of time and distance constraints. The manual nature of the radar analysis methods was quite time consuming (as described in section 2.3). Applying this final guideline helped expedite the radar analysis approach, while also accounting for, and including, rapid changes to system characteristics revealed by WSR-88D imagery.

## 2.3. Assessment of Ingredient #1: Shear/Cold Pool Balance

As discussed in Section 1.2, the first ingredient of the 3-I-M approach attempts to assess the relative balance of horizontal vorticity rotors generated by a system cold pool and ambient environmental shear. SP12 notes that a lack of operationally available, efficient, and accurate means to assess the strength/depth of system cold pools facilitates the need to approximate this "ingredient" via alternate approaches. A commonly applied operational approach is to assume that a system is "balanced" (in the RKW sense) when convective updrafts are located close to the leading edge of the cold pool. This balance is assessed by utilizing both 2-D plane view and horizontal cross-sections of WSR-88D imagery/dual-pol products to assess the balance regime(s) of the QLCS. Examples of both approaches are shown as Figures 8 & 9. While either approach may prove relatively quick and practical in operations, especially for experienced forecasters, it introduces substantial subjectivity to this component of the 3-I-M. Therefore, a secondary goal of this study is to develop an objective and operationally reproducible approach to quantify the shear/cold pool balance of a given system. One often identifiable QLCS feature (via radar assessment) is the Updraft Downdraft Convergence Zone (UDCZ), a proxy for the leading edge of the cold pool/gust front. Using the UDCZ position, the approach of this report was to compare the distance between this feature and threshold reflectivity values associated with the leading

convective line. Distances were computed using three different reflectivity values: 40, 45 and 50 dBZ, given ambiguity in how the leading edge of the convective line should be defined. Past studies applying radar-based interrogation of QLCSs have highlighted similar threshold values to represent the convective cores of the system (Parker et al. 2000, Haberlie and Ashley 2019). In addition to calculating the UDCZ-to-reflectivity (U-to-R) distance using the 40, 45, and 50 dBZ thresholds, an "All" dBZ and dBZ gradient distance was also calculated along the convective line of the QLCS. The "All" dBZ (henceforth AdBZ) measure was an arithmetic average of the U-to-R distances using the 40, 45, and 50 dBZ thresholds at each analysis point. The dBZ gradient measure was the difference between the UDCZ-to-40 dBZ and UDCZ-to-50 dBZ distance at each point of analysis. The reflectivity gradient was computed to assess the potential utility of this measure in identifying more vertically upright convection.

The first step in assessing the distance between UDCZ and dBZ thresholds is determining the UDCZ position at valid radar analysis times (discussed in section 2.2). An example of the four-panel radar visualization used to determine the UDCZ position (in GR2Analyst) is shown as Figure 10. Radar variables in the four-panel visualization include: reflectivity (Z), base velocity (BV), storm relative velocity/motion (SRV/M) and spectrum width (SW). Schaumann and Gagan (2013) highlight this radar workstation visualization, and utility of spectrum width and storm-relative motion products, in determining the position of the UDCZ.

The initial step in calculating the U-to-R distance was determining the portion of the convective line to be analyzed. This applied the radar analysis criteria discussed in Section 2.2. The motion vector of the UDCZ was determined using the interactive storm motion/speed tool within the GR2Analyst software. This was done by comparing the previous position of the analysis point along the UDCZ and extrapolating it forward (visually) to the next analysis time

(full volume scan) of interest. An example showing the outcome of estimating storm motion and application of the storm motion/speed path (white line) is shown in Figure 11. The distance between the analysis "point" (i.e. UDCZ) position and threshold reflectivity values were then measured (using cursor readout in GR2Analyst) along the applied path. Moving from the analysis point inward toward the main convective line (i.e. opposite of storm motion) was represented as a positive (+) distance. Conversely, moving from the UDCZ analysis point away from the convective line (i.e. in direction of storm motion) was represented as a negative (-) distance. A broad overview of this process is shown as Figure 12.

The process described above (estimate local UDCZ motion, apply storm motion path, measure U-to-R distance) was repeated at intervals of 15 km along the convective system major axis during valid analysis times. Additional analysis points, at 15 km intervals, continued until either 1) the next point lied outside the 100 km maximum radial distance from the single-site radar of use and/or 2) the convective line ($\geq$ 40 dBZ echoes) reached the radar (or launch) site. An example of added analysis points, where U-to-R distances were calculated, from the 28 August 2018 case across northern Michigan, are represented as points "A" and "C" in Figure 13.

This methodology step yielded a collection of individual points along the convective line where U-to-R distances were calculated during each valid analysis time/volume scan. In order to approximate the first "ingredient" of 3-I-M over the broad spatial extent of each study QLCS, U-to-R measures at adjacent points (15 km spacing) were combined to create "segments". Figure 14 shows an example of this process. The U-to-R distances, using each dBZ threshold, from each point included in a segment were (arithmetically) averaged and made to represent the 15 km line-segment spanning the two points. While variability in the U-to-R distance can occur over spatial scales smaller than 15 km, this approach was deemed sensitive enough to capture the variability

13

of this measure across the QLCS, while also balancing against the overall time burden of this analytical approach.

In total, 1,820 unique line segments were created among the 50 study QLCS events. Due to radar "artifacts" occurring at certain analysis points (discussed below), a smaller subset (1,234) of segments includes all five U-to-R calculations discussed above. An additional 561 segments are missing at least one (i.e. 40, 45, 50, AdBZ, dBZ gradient) calculated measure. Only 25 segments contain no U-to-R distance measurement, primarily owing to radar beam blockage (due to enhanced terrain) at certain WSR-88D/QLCS event locations.

At certain analysis points, so-called radar "artifacts" made calculating U-to-R distance more complex. Examples of these radar artifacts are shown as Figures 15 & 16. Figure 15 represents what the authors termed "enhanced reflectivity", or regions of pre-UDCZ/convective line enhanced ($\geq$ 40 dBZ echoes) stratiform precipitation. At these analysis points (ex. Point 'P' on Figure 15) the U-to-R distance using the 40 or 45 dBZ threshold could be met moving either left or right along the calculation path.

An additional radar artifact that was noted throughout the radar analysis was single/multi-cell convection initiating immediately ahead of the advancing UDCZ/gust front. An example of this behavior is shown in Figure 16, where single-cell convection, clearly independent of the advancing convective system, intersected the U-to-R calculation path (i.e. white line in Figure 16). Again, this behavior allows for threshold values to be met by moving either left or right along the calculation path.

Whether the convective system helps promote the existence of these radar artifacts is open for additional discussion; they were treated as independent features during the analysis process. To isolate echoes within the primary convective system of interest, the U-to-R distance

to the first ≥ 50 dBZ echo, clearly associated with the convective system, was calculated and cataloged. The use of spectrum width and storm-relative velocity/motion products, along with assessing the overall time evolution of reflectivity (Z), helped in properly assessing the appropriate direction of measurement along the calculation path. At analysis points where this measurement approach was employed; 40, 45, AdBZ and dBZ gradient measures were not calculated. When creating line segments for analysis, should one of the two analysis points used to create the segment only contain a ≥ 50 dBZ measurement (due to radar artifacts) then the ≥ 50 dBZ U-to-R distance would be the only measure for that segment.

A few caveats within the methodological approach to quantify the shear/cold pool balance deserve additional discussion. One obvious caveat is representing the UDCZ as (straight) line segments over the length of the QLCS. In reality, as can be seen in Figures 6 & 7, the UDCZ often takes on unique orientations across small spatial scales (i.e. smaller than 15 km). Another caveat in this approach are small time and distance-based discrepancies that can exist when using multiple polarimetric variables in concert with each other. This was noted when trying to calculate U-to-R distances, the fundamental approach in this method. The position of the UDCZ was primarily assessed using spectrum width and storm-relative velocity/motion. These products have a slightly longer processing time lag when compared to reflectivity imagery over each volume scan. This has a downstream impact when attempting to compare the position of the UDCZ and enhanced reflectivity using differing dual-polarimetric products.

## 2.4. Assessment of Ingredient #3: Rear-Inflow Surges

As discussed in Section 1.2, the third ingredient of the 3-I-M assesses surges or bows within the convective line, hypothesized to be induced by a RIJ or enhanced outflow. Similar to assessment of the first "ingredient", analysis of rear-inflow surges over the 50 studied QLCS

events was conducted via a manual radar analysis process. The method(s) to assess surge/bow signatures took place over concurrent radar images used for assessment of the first "ingredient" (Section 2.3).

For this report, rear-inflow surges were assessed in comparing previously created line segments (Section 2.3) to the configuration of wind fields revealed by base and storm-relative velocity imagery. More specifically, the orientation of line segments (a proxy for the UDCZ/gust front position) was compared to the nature of rear-to-front flow across the segment. An example of this process is shown as Figure 17. As is noted along segment 'AB' in Figure 17, the rear-to-front flow (inbound wind towards the KAPX WSR-88D) caused a concavity to the otherwise straight line segment (i.e. UDCZ appears "bowed out"). Identified zones of enhanced rear-to-front flow across individual line segments were denoted as "local surges", with the apex of the surge (in a line segment relative sense) noted by its latitude/longitude coordinate pair.

It became apparent in assessing local rear-inflow surges that broader expanses of enhanced rear-to-front flow would become "washed out" if compared to individual line segments. For example, the leading edge of a larger rear-inflow surge is denoted as the white line in Figure 17. This surge was roughly aligned along the edge of segment 'BC'. This induced little signal for a rear-inflow surge in following the approach for identifying local surges. Therefore, for these large expanses of enhanced rear-to-front flow, the relative apex was independently (irrespective of segment) and subjectively assessed. Once determined, the position (latitude/longitude pair) of this "broad" surge was tied to the segment that contained its apex.

A few caveats within the surge analysis approach deserve additional discussion. The first being that individual analysis segments may contain both a 'local' and 'broad' surge, despite the feature being more coherent (i.e. not two different types of surges). An example of this is shown

from the 28 August 2018 QLCS case, where segment 'AB' contains the apex of both a local and broad surge, despite evidence of one (broad) surge extending across portions of segments 'AB' and 'BC' (Figure 17). Another caveat in determining rear-inflow surges was previously identified in the approach to assess the first 3-I-M ingredient (Section 2.3). Namely, using the created (straight) line segments to determine enhanced rear-inflow. The approach applied introduces the possibility that features quantified as surges are more attributable to heterogeneities in the overall structure of the UDCZ/gust front, rather than solely from rear-to-front flow. A previous 3-I-M study, conducted at the NWS in Springfield, MO, followed a similar process to note rear-inflow surges. This study quantified rear-inflow surges as "displacing the original UDCZ ≥ 4 nm". The ≥ 4 nm threshold was measured from the assumption of a "straight" (i.e. north-south) UDCZ (Jason Schuamann, personal communication). While no distance criteria was applied in this report, the idea of quantifying rear-inflow surges as regions where rear-to-front flow perturbs an otherwise "straight" UDCZ is consistent with this approach.

## 2.5. Assessment of Ingredient #2: Quantifying 0-3 km Bulk Wind Shear

The second 3-I-M "ingredient" for QLCS mv-genesis is the line-normal component of bulk wind shear from the surface to 3 kilometers (0-3 km) above ground level (AGL) at or exceeding 30 knots. In this study, bulk wind shear vectors in the 0-3 km depth were calculated using raw (QC'ed) wind data from the (50) individual proximity soundings tied to the QLCSs of study. Wind (sounding) data from the 9 proximity soundings, associated with observed field program QLCSs, was accessed via the Earth Observing Laboratory (EOL) platform in ASCII file format. Sounding datafiles from the remaining 41 proximity soundings, associated with

operational launches conducted by the National Weather Service, were accessed via the National

Center for Environmental Information (NCEI) archive in text file format.

Multiple calculation approaches were conducted to quantify the 0-3 km bulk wind shear

(henceforth 3Shear) vectors. The first approach simply subtracted the 10-m wind vector from the

3-km wind vector (interpolated linearly to 3-km). This approach was colloquially noted as the

"two-point" method. Two additional approaches in determining 3Shear vectors were tested. The

first, termed as the "layer average" method, used the average wind vector between the surface

and 250 meters AGL as the bottom vector, and the average wind vector between 2750 and 3250

meters AGL as the top vector. The final method, called the "10 meter + layer averaged" method,

used the surface (10 meter) vector as the bottom vector and the averaged vector between the

2750 and 3250 meters AGL as the top vector. Figure 18 displays a KDE distribution of 3Shear

from the three different calculation approaches. Given limitations in data/wind resolution in four

operational soundings, along with similar distributions of 3Shear across all approaches (Figure

18), the "two-point" method was used in this report.

As discussed previously, the 3-I-M calls for assessing the magnitude of 3Shear **normal** to

the convective line. Previous operational attempts to assess the line-normal component of

3Shear, such as those discussed in SP12, compare broad portions of the convective line to

model/observed 3Shear vectors. In this study, the novel technique of creating 1,820 unique line

segments for the 50 study cases allowed for line-normal shear components to be assessed at a

higher spatial resolution within the line than previous studies (i.e. SP12). To determine the line-

normal component of 3Shear, the orientation/direction of each segment was compared against

the previously identified 3Shear vector. The orientation of each line segment was determined

using the Haversine formula, which calculates the distance between two latitude/longitude

points. The Haversine formula is shown as Eq. 1

$$\theta = tan(sin(\lambda_2 - \lambda_1) \cdot cos(\varphi_2), cos\varphi_1 \cdot sin\varphi_2 - sin\varphi_1 \cdot cos\varphi_2 \cdot cos(\lambda_2 - \lambda_1)) \quad \textbf{(Eq. 1)}$$

Where $(\varphi_1, \lambda_1)$ and $(\varphi_2, \lambda_2)$ represent the latitude/longitude pairs of points at the end of each line

segment. Using determined line segment orientations, the line-normal component of 3Shear was

then computed. Sine and cosine concepts were then applied to determine the line-normal wind

shear component across each line segment.

## 2.6. Radar Assessment of Mesovortices

Identifying mv-genesis events within the 50 study QLCSs was critical in order to test the

utility of 3-I-M concepts. A criteria for identifying MVs, via radar interrogation, was developed

in personal communication with NWS Springfield, MO Science and Operations Officer Jason

Schaumann, co-author in the SP12 manuscript. In order to be categorized as an MV in this

report, the following three conditions had to be met:


1.) Rotational velocities (VROTs) ≥ 20 knots

2.) Extend across a vertical depth of ≥ 8000 feet

3.) Persist at least 2 full volume scans.


This criteria was proposed by NWS Senior Forecaster Ron Pryzbylinski, and has been used in

both operational and research settings. Previous studies have applied similar approaches to

define vortex-like structures via WSR-88D data interrogation (Smith et al. 2015; Sessa and

Trapp 2020). Qualitatively, this criteria follows the findings of Atkins (2004), which describes

tornadic MVs as being "longer-lived and stronger at low levels" and deepen rapidly prior to

tornadogenesis. In applying the above criteria, 42 unique MVs were identified across 21 of the 50 study QLCSs.

During the radar analysis of MVs, multiple rotational signatures were identified that failed to meet at least one of the MV conditions. A unique criteria was applied to include these weaker/shorter-lived signatures, termed "transient mesovortices" (MVTs), in the analysis. MVT criteria was defined as rotational signatures meeting at least one of the following conditions:

1.) Rotational velocities (VROT) $\leq 20$ knots

2.) Extend across a vertical depth of $\leq 8000$ feet

3.) Persist only 1 full volume scan

Applying the MVT criteria led to the identification of 47 unique MVT signatures across 27 of the 50 study cases.

# Chapter 3: Verification of 'Three-Ingredients' Method

## 3.1. Distribution of Bulk and Line-Normal 0-3 km Wind Shear

At the onset of the analysis, distributions of bulk and line-normal 3Shear were calculated to determine trends of the second 3-I-M ingredient across all 50 study QLCSs. Figure 19 shows the distribution of bulk 3Shear magnitudes calculated from the 50 proximity soundings using a kernel density estimation (KDE). The peak in the distribution was ~30 kt, with a longer distribution tail towards higher values (Figure 19). A KDE distribution of line-normal 3Shear measured across all 1,820 segments is displayed in Figure 20. The peak in the distribution is well below (by 8-10 kt) the 30 kt threshold value for mv-genesis ascribed in the 3-I-M. A final KDE distribution of line-normal 3Shear, for segments that observed mv-genesis, is shown in Figure 21. Similar to the line-normal 3Shear over all segments, mv-genesis segments (n = 37) have a peak in distribution below the 30 kt threshold 3-I-M value. There is also evidence of a secondary "peak" in the distribution around ~50 kt. The outcomes displayed in Figure 21 present a significant early finding that **mv-genesis events occurred for values of subcritical (from the 3-I-M approach) line-normal 3Shear**. Finally, Figure 22 displays all three above KDE distributions together. In general, the distribution of line-normal shear magnitudes trended slightly higher for mv-gen segments than for all segments.

## 3.2. Comparison of Shear/Cold Pool Balance and 3Shear

As discussed in Section 1.2, the first and second 3-I-M ingredients are physically connected. Ingredient #1, or a shear/cold pool in a "balanced" or "slightly shear dominant" regime, is theorized to be favored when Ingredient #2, or the line-normal 3Shear, is $\geq$ 30 knots. Therefore, direct comparison of the first two ingredients can help illustrate the relative strength of the theorized relationship.

As captured by the regression plot of Figure 23, the U-to-R distance using the 40 dBZ threshold was compared to line-normal 3Shear. Each segment containing a valid 40 dBZ distance and value of line-normal 3Shear (1,403 segments) were included in Figure 23. Overall, a weak negative correlation ($R^2 = -0.33$) is evident in this approach to quantifying the first and second ingredient. Physically, weak signal exists in calculated line-normal 3Shear and the corresponding shear/cold pool balance regime. Additionally from Figure 23, 93% (28/30) of mv-genesis segments (red scatterers) observed a 40 dBZ-to-UDCZ distance between -5 to 2 km. Physically, this represents updraft towers (using the 40 dBZ quantification) lying 2 km behind to 5 km ahead of the UDCZ for ~93% of mv-genesis events in the dataset.

Additional linear regression plots were created to assess the shear/cold pool balance relationship using the 45, 50, AdBZ, and dBZ gradient U-to-R thresholds. (Figures 24-27). This included 1,393, 1,626, 1,234, and 1,234 individual segment measures respectively. Using alternative U-to-R thresholds continued to yield weak (negative) linear correlation ($-0.27 > R^2 > -0.34$) in comparison of the first two 3-I-M ingredients. Mv-genesis segments, across all additional shear/cold pool balance quantifications, continued to observe reflectivity-to-UDCZ distances generally between -5 to 5 km. This reinforces a potential (objective) U-to-R distance range to describe a favorable shear/cold pool balance for mv-genesis.

### 3.3. Isolating Line-Normal 0-3 km Wind Shear

Provided that subcritical magnitudes of line-normal 3Shear were observed for numerous mv-genesis segments (Section 3.1), this ingredient was isolated to determine possible differences between mv-genesis and "null" segments. Line-normal 3Shear magnitudes across transient mv-genesis and segments that did not produce mesovortices (referred to as "null" segments) were

also assessed.  Boxplots for comparing mv-genesis (and "transient" mv-genesis) against null segments is shown in Figure 28.

Most notable from the left panel of Figure 28 (mv-genesis segment comparison), the mean and median of line-normal 3Shear magnitudes across mv-genesis segments lies just above the 30 kt 3-I-M threshold. Additionally, a significant overlap exists between the 25-50th percentile of  mv-genesis segments and the 50-70th percentile of null segments. Even weaker differentiation (i.e. more overlap) in line-normal 3Shear is apparent between transient mv-genesis and null segments (right panel of Figure 28). Not only does the mean and median of transient mv-genesis segments lie beneath the 3-I-M threshold, there is even greater overlap between segment outcomes. This has significant ramifications on the utility of using the wind shear 3-I-M ingredient as a discriminator for favorable mv-genesis environments/segments.

## 3.4. Rear-Inflow Surge Impact

The third ingredient of the 3-I-M is the presence of a surge or bow along the convective line. Assessing the prevalence of these features, relative to observed MV and MVTs, is shown in Figures 29 and 30 respectively. Both figures (scatterplots) include similar base components, though the scatterers of Figure 29 represent mv-genesis segments, while transient mv-genesis segments are displayed in Figure 30. As presented in Figure 29, surge/bow features were present for a majority of mv-genesis events, extending across a wide spectrum of first (50 dBZ-to-UDCZ distance) and second (line-normal 3Shear) ingredient regimes. The 50 dBZ-to-UDCZ distance was chosen to represent the shear/cold pool balance (first ingredient) in this analysis owing to radar "artifacts" (Section 2.3) preventing full suites of distance measures across all mv-genesis segments. The overall relationship of enhanced surge/bow outcomes, relative to assessed MVTs,

was much more disparate than that of MVs. Approximately 50% of MVTs occurred without the presence of an apparent enhanced surge/bow along the line segment of generation (Figure 30).

## 3.5. Using Additional Shear Depths

Recent observational analysis studies have identified that wind shear across different/varying vertical depths may help in the mv-genesis process. Flournoy & Coniglio (2019) analyzed trajectories of parcels that populated a simulated (tornadic) mesovortex using in-situ observations from the PECAN field campaign on 6 July 2015. One parcel pathway identified was low-level (100-300 meters AGL) inflow parcels from the ambient environment. Very strong vertical wind shear, oriented parallel to the gust front, generated crosswise horizontal vorticity that was then tilted by a local outflow surge and then populated the nascent mesovortex updraft. Given this finding, it appeared appropriate to assess whether low-level wind shear (1 km AGL) and its configuration (line-parallel) showed utility in discriminating mv-genesis potential. Additionally, given the 3-I-M approach to assess the wind shear that promotes favorable shear/cold pool balance, the line-normal component of shear in the lowest 1 km was also studied given that cold pools can be shallower than 3 km, especially for events in the Southeastern United States (Sherburn et al. 2014).

The line-normal and line-parallel components of 0-1 km AGL bulk wind shear (henceforth 1Shear), over all segments, were compared against shear/cold pool balance distances and mv-genesis outcomes to assess for a discriminatory signal. Given broadly analogous trends across all dBZ thresholds, and for the sake of brevity, the line-normal and parallel components of 1Shear are compared against shear/cold balance using the 50 dBZ U-to-R threshold value. The comparison of line-normal 1Shear versus 50 dBZ-to-UDCZ distance is shown in Figure 31, while the line-parallel component is displayed in Figure 32. Namely, a weak (negative) linear

relationship is evident when using either component of 1Shear to parameterize the second

ingredient and compare to associated shear/cold pool balance over the segment. These follow the

trends revealed by the original 3-I-M approach using wind shear in the 0-3 km AGL depth

(Section 3.3), with no clear indication that line-parallel or line-normal shear over 1 km

discriminates differently than 3Shear for mv-genesis. However, focusing on the red scatterers of

Figures 31 & 32, representing mv-genesis segments, a few additional takeaways are evident

when applying 1Shear. Most notably, a large proportion of mv-genesis segments observed 0-20

knots of line-normal and 10-30 knots of line-parallel 1Shear. More broadly speaking > 0 knots of

line-normal and > 10 knots of line-parallel shear were observed for mv-genesis segments in the

study dataset (Figures 31 & 32). This suggests that mesovortices require at least some line-

normal low-level flow/shear that is oriented rear-to-front (relative to the orientation of the gust

front). The bottom threshold of 10 kt for the line-parallel shear might be used as a lower limit for

when mesovortices can be expected. However, it may simply reflect that QLCSs tend to occur in

environments of enhanced low-level flow from nocturnal boundary layer processes or in the

warm sector of larger-scale cyclones that force stronger flow aloft through baroclinic processes.

Another characteristic of an environment that can maintain favorable shear/cold pool

alignment despite weaker low-level shear, is the presence of deep-layer shear, which is often

present in QLCS environments. For example, Cohen et al. (2007), highlighted the utility in using

deep-layer shear (commonly measured in the surface to 6 km AGL layer) to quantify the overall

severity of linear convective systems. Cohen et al. (2007) found that greater magnitudes of deep-

layer shear, orthogonal to the primary convective line, provided greater distinguishing power at

quantifying QLCS severity/strength than did shear within shallower depths (Figure 33).

Physically, the updraft-in-shear concept applied to nearly two-dimensional convective systems

(Parker 2004), acts to maintain convective updrafts close to the leading edge of the gust front (Coniglio et al. 2006). This may explain why greater magnitudes of deep-layer shear help enhance QLCS strength. Figure 34 depicts a schematic of the updraft-in-shear concept. The pressure perturbation deficit (downshear of deep-layer shear vector) across an updraft provides the lift necessary to establish deep updrafts that may amplify the tilting and stretching of vorticity along the convective system gust front. This is theorized to occur atop the cold pool of an evolving convective system.

In concert with the discussion of evaluating 1Shear, the impact of using 0-6 km AGL bulk wind shear (henceforth 6Shear) as a modified 3-I-M wind shear ingredient was assessed. Once again, a visualization of the relationship between the modified wind shear approach and analyzed shear/cold pool balance is shown in Figure 35, capturing line-normal 6Shear against the 50 dBZ U-to-R distance. While the overall (negative) linear relationship remains relatively weak ($R^2 = (-)0.33$), 6Shear observed the "strongest" quantification of the shear/cold pool balance amongst all shear configurations and depths tested ($(-)0.42 < R^2 < (-)0.33$) . In general from Figure 35, segments that observed mv-genesis (red scatterers) observed $\geq 20$ knots of line-normal 6Shear. Isolating line-normal 6Shear magnitudes (Figure 36) shows pronounced separation when binning outcomes based upon mv-genesis. The mean and median of 6Shear magnitude for segments with identified mv-genesis lie well outside (above) the 75th percentile for segments that did not.

## 3.6. Comparing Surge and Shear Combinations

The effect of rear-inflow surges, regardless of triggering mechanism or relative size, over the 50 study QLCS cases were discussed in Section 2.4. While not explicitly described in the original 3-I-M approach/SP12, line-normal wind shear magnitudes (at all depths tested) were

compared against presence of rear-inflow signatures to determine possible mv-genesis discriminating power. This is similar to Gibbs (2021) which tested combinations of system and environmental variables to maximize detection of mv-genesis events. Figures 37 & 38 display wind shear magnitudes for segments that contained a rear-inflow surge, binned by mv-genesis, for line-parallel and line-normal 1Shear, line-normal 3Shear, and line-normal 6Shear respectively. Broadly, varying depths and configurations of environmental wind shear, in the presence of bowing structures, showed weak ability to differentiate between mv-genesis outcomes (Figures 37 & 38). Line-normal 6Shear showed most utility (though still overall weak) in differing mv-gen potential across surge segments (right panel of Figure 38). The mean and median of line-normal 6Shear for mv-genesis segments was slightly higher than the 75th percentile of non-mv-genesis segments. Using bulk wind shear (across varying depths) in combination with rear-inflow surges shows weak utility for real-time operations.

## 3.7. Assessment of Thermodynamic Variables

Though not explicitly defined in the original 3-I-M, thermodynamic variables can serve as valuable discriminators for severe weather and QLCS environments (Thompson et al. 2012; Anderson-Fry et al. 2016; Rogers et al. 2016) In this report, thermodynamic variables were assessed from proximity sounding output. Visualization of sounding profiles, and associated thermodynamic variables employed the SHARPPy sounding package. Given spatiotemporal limitations of thermodynamic measures (i.e. single value from proximity sounding), assessment occurred broadly over the 50 study cases (by mv-genesis and tornadic mv-genesis outcomes) as opposed to the segment-by-segment approach of Sections 3.1-3.6. Given the sample size of cases (50), mv-genesis (42), and tornadic mv-genesis (9) events, discussion of outcomes in this section

should be treated as preliminary in nature, but provide possible hypotheses to test using past and future observational datasets.

In operational settings, application of the 3-I-M includes analysis of radar signatures and environmental conditions that have been identified as potential mv-genesis precursors. Termed "confidence builders" and "nudgers" by WDTD guidance, the presence of certain radar and environmental signatures are intended to raise forecaster situational awareness to a tornadic MV threat. One so-called "nudger" is the presence of $\geq 40$ J/kg of mixed-layer convective available potential energy (CAPE) in the surface to 3 km AGL layer (henceforth 3CAPE). This variable was assessed from each proximity sounding tied to study QLCS events. Figure 39 shows box-and-whisker plot comparisons of 3CAPE across all cases, subdivided by mv-genesis (left) and tornadic mv-genesis (right) events. As evident in Figure 39, a rather significant overlap exists for the mean value (and percentile ranges) of 3CAPE for mv-genesis and tornadic mv-genesis events relative to null cases.

An additional thermodynamic variable tested was the lifted condensation level (LCL) using the mixed layer parcel (henceforth MLLCL). Physically, the MLLCL is representative of cloud base height when lifting the mean parcel contained in the bottom 100 mb of the troposphere. Study of this thermodynamic variable was motivated by observational analysis during the Propagation, Evolution and Rotation in Linear Storms (PERiLS) Field Program in the Spring of 2022. Of particular interest was a QLCS that propagated across the Mid-Mississippi Valley during the afternoon of 13 April 2022. Proximity soundings released by the National Severe Storms Laboratory (NSSL) Lidar Team showed MLLCL values around 1300 meters AGL (Figure 40). Yet, as confirmed by NSSL and NWS damage survey teams, three QLCS mesovortex tornadoes occurred <1 hour/<50 km to the west-southwest of the NSSL Lidar

28

position across far northeastern Arkansas into southern Missouri bootheel (Figure 41). While rapid environmental-scale changes have been observed in past observational severe convective studies (Sherburn and Parker 2014; King et al. 2017), the spatiotemporal proximity of the sounding to the convective system presents an interesting outcome to test in this report.

Again, MLLCL values from the 50 proximity soundings/cases were binned based upon observed mv-genesis (left panel) and tornadogenesis (right panel) outcomes (Figure 42). A key takeaway from the right panel of Figure 42 is that the mean and median of MLLCL heights for cases that observed at least one tornadic MV lie at (or just below) the 25th percentile for non-tornadic cases. Physically, lower cloud bases (when lifting the mixed-layer environmental parcel) were favored for QLCS cases that observed at least one tornadic MV in the dataset. Additionally, all MLLCL values (i.e. cloud base heights) for tornadic MV cases were <800 meters AGL. Past findings (Thompson et al. 2003; Kirkpatrick et al. 2007) have identified that regimes of lower MLLCL heights favors tornadogenesis. While sample size (n = 9) introduces uncertainty in the discussed outcome, it presents an interesting hypothesis to test in future work.

A final thermodynamic variable assessed was the temperature lapse rate over the lowest 1 km AGL (henceforth 0-1LR) ahead of each convective system. Previous studies, mostly notably Sherburn and Parker (2014), highlighted the utility of using temperature lapse rates over the 0-3 km AGL depth to distinguish between environments favorable for severe weather in high shear/low CAPE (HSLC) environments. Based upon this work, in addition to the understanding of plausible mv-genesis mechanisms (enhanced low-level tilting and stretching), low-level lapse rates (0-1LR) were tested across the 50 study events.

Unlike the previous thermodynamic variables, the 0-1LR was not determined (i.e. not calculated) using the SHARPpy sounding software package. This facilitated the need to calculate the 0-1LR value using the raw (QC'ed) sounding data and applying Eq. 2

$$\Gamma_1 = \frac{T_1 - T_0}{1\ km} \quad \textbf{(Eq. 2)}$$

where $\Gamma_1$ represents the 0-1LR, $T_0$ represents the dry-bulb temperature at the surface, and $T_1$ represents the dry-bulb temperature at 1 km AGL. Eq. 2 was inputted into a Python programming script and executed for data from each proximity sounding. Again, for the 41 "operational" soundings (i.e. lower vertical/time resolution), a linearized dry-bulb temperature value at 1 km AGL was computed. Figure 43 represents a comparison boxplot of 0-1LR for mv-genesis (left) and tornadic mv-genesis (right) outcomes. Both panels of Figure 43 elucidate that 0-1LR provide limited utility in discriminating between mv-genesis and tornadic mv-genesis environments for cases in the study dataset.

## 3.8. Comparing 0-3 km Line-Normal Vs. 0-1 km Line-Parallel Wind Shear

Based upon past observational analysis, a combination of previously discussed variables were compared to determine the overall utility in discriminating QLCS mesovortex environments. Namely, in regimes of sub-critical (line-normal) 3Shear, do increased magnitudes of line-parallel 1Shear compensate to aid in mv-genesis? Figure 44 shows a representation of this shear comparison. Given the nearly horizontal regression line, a weak relationship exists between these shear variables/depth. Given the multiple potential pathways for MV-populating parcels, identified by Flournoy and Coniglio (2019), this outcome is not wholly unsurprising.

# Chapter 4: Discussion and Conclusion

This report used 50 observed Quasi-Linear Convective Systems (QLCSs) to evaluate the 'Three-Ingredients' Method (3-I-M) for forecasting QLCS mesovortices (MVs). Developed by Schaumann and Pryzbylinski (2012), the 3-I-M assesses a combination of both internal and external system characteristics to aid in early identification of mesovortices (and associated tornadic threat). *The first ingredient of the 3-I-M is met when ambient environmental shear and the system cold pool are said to be "balanced" or "slightly shear dominant".* Vertically deep and upright updrafts (enhanced tilting and stretching potential) are favored in these shear/cold pool balance regimes (Rotunno et al. 1988, Weisman and Rotunno 2004). The shear/cold pool balance of each system was assessed by measuring the distance between the updraft downdraft convergence zone (UDCZ) and elevated reflectivity (Z) thresholds within the convective line. Measurements were taken every 15 km along the major axis of the system. *The second 3-I-M ingredient is line-normal wind shear magnitudes, in the bottom 3 kilometers of the atmosphere, of at least 15 m s$^{-1}$ (30 knots).* This magnitude of line-normal 0-3 km wind shear (3Shear) is hypothesized to promote the favorable shear/cold pool balance regime. Wind shear magnitudes were assessed using raw wind data/vectors from field campaign and operational soundings launched in proximity to each study QLCS. *The third 3-I-M ingredient is the presence of a bow or surge of the main convective line, generally resulting from enhanced outflow or rear-to-front flow.* Though the physical significance of this ingredient remains unresolved, rear-inflow jets have been identified as a plausible mv-genesis mechanism by Xue et al. (2015) and Flournoy and Coniglio (2019). A subjective radar analysis was employed to determine the presence of rear-inflow surges amongst the study cases. Where these three ingredients overlap along a convective line favors the generation of mesovortices (and tornadoes) using the 3-I-M approach. Finally,

MVs were (subjectively) assessed across all cases using an operational criteria developed by NWS senior forecaster Ron Pryzbylinski. This criteria has been used in a National Oceanic and Atmospheric Administration funded undergraduate research project testing the 3-I-M, and contains similar components to previous radar-based studies assessing vortex-like signatures (Smith et al. 2015, Trapp and Sessa 2020).

A key finding in this report is that mv-genesis events (~46%) were observed in regimes of line-normal 3Shear below the 3-I-M threshold (i.e. 30 knots). In addition, shear within the 0-3 km layer showed a weak relationship against the shear/cold pool balance concurrently assessed. These results agree with Bryan et al. (2005) that the cold pool often varies in depth (strength), and applying an approximation of 3 km appears suspect across a wide continuum of geographic and seasonally disparate QLCS events. While this report does not address ways to assess cold pool depth/strength in operational settings, assessing wind shear within the 3 km depth ascribed by the 3-I-M may prove unreliable as a one size fits all approach to determine the shear needed for a favorable balance regime.

Contrary to the shortfalls identified in assessment of line-normal 3Shear, both shear/cold balance, and the presence of rear-inflow surges, appears to indicate favorable conditions for mv-genesis. While a wide variety of UDCZ-to-reflectivity distances (shear/cold pool proxy) existed across study cases (and analysis segments), a distance range of -5 to 5 km was generally assessed for segments in which mv-genesis was observed. A negative distance refers to a "shear dominant" outcome, where the UDCZ lies behind of the convective cores. A positive distance refers to a more "balanced" outcome, where the UDCZ lies just ahead of updraft towers. This offers the potential to redefine the first ingredient in the 3-I-M approach using an objective criteria that can be readily applied in operational settings.

Additionally, the correlation between rear-inflow surges and observed MV outcomes within this report confirms the importance of these features in promoting mv-genesis (Atkins and St. Laurent 2009a,b; Trapp and Weisman 2004). Once again, the ability to readily identify these features through radar analysis provides an opportunity to immediately apply this finding in operational settings. While the radar analysis conducted to identify surges was subjective in nature, extensive operational guidance currently exists to identify these features in warning decision settings.

Findings of Flournoy and Coniglio (2019) and Cohen et al. (2007) facilitated the investigation of wind shear contributions to mv-genesis across both shallower and deeper atmospheric depths. Both the line-normal and line-parallel component of wind shear in the lowest 1 km AGL (1Shear) provided weak signal for mv-genesis outcomes and relationship to shear/cold pool balance. One potentially operationally relevant result was that nearly all (~97%) of MV cases occurred with positive (> 0) magnitudes of line-normal 1Shear. Again, in operational settings, this variable can be assessed by upper-air, vertical wind profile (VWP), or model guidance output of 0-1 km shear vector orientation relative to the convective line of interest.

The line-normal component of deep-layer (0-6 km) shear (6Shear) was also assessed. While slightly better than applying the 0-1 and 0-3 km layers, wind shear within the deeper depth yields overall weak discriminatory signal in both shear/cold pool balance regime and overall propensity to generate MVs. Similar to the outcomes of line-normal 1Shear, some signal existed in defining a lower boundary of line-normal 6Shear favorable for mv-genesis. This lower boundary magnitude was approximately 20 knots.

While not explicitly defined by the original 3-I-M framework, a small subset of thermodynamic variables were assessed to test for discriminatory signal in mv-genesis outcomes. The first variable tested was the mixed-layer convective available potential energy in the lowest 3 km AGL (3CAPE). Operational (NWS) guidance, utilizing the 3-I-M for warning decision support, identifies ≥ 40 J/kg of 3CAPE as a threshold to increase forecaster confidence in issuing an MV-related tornado warning. There is relatively significant overlap (minimal discrimination) of measured 3CAPE magnitudes when subdividing events by both MV and tornadic MV occurrence. The low-level (0-1 km AGL) temperature lapse rate and lifting condensation level of the mixed layer parcel (MLLCL) were also tested. Both variables generally showed overall weak ability in identifying favorable mesovortex producing QLCSs and tornadic MV potential within study cases. One standout outcome was comparing the MLLCL for tornadic and non-tornadic MVs. Tornadic MVs in the dataset were observed in regimes of significantly lower MLLCLs heights, agreeing with previous studies of tornadic convection (Thompson et al. 2003; Kirkpatrick et al. 2007).

# Chapter 5: Operational Recommendations

The primary motivation of this report was to evaluate the 3-I-M using a large dataset of observed cases, identify scenarios where it failed to capture/predict a mesovortex (tornado) threat, and develop operational recommendations for such "failure mode" events. In using the native 3-I-M, authors note continued application of rear-inflow/surge/bow identification as a strong precursor signal for mv-genesis potential. Additionally, this report has introduced an objective threshold to quantify the shear/cold pool balance of systems (i.e. UDCZ-to-updraft tower distance) which can be assessed in operational settings. As discussed in multiple sections of this report, assessment of bulk wind shear in the 0-3 km layer shows the most significant shortfall in applying the original 3-I-M. While this report does not identify an appropriate depth of wind shear to apply in its place, threshold values of shallow (0-1 km AGL) and deep-layer (0-6 km AGL) line-normal shear **may** exist ($\geq 0$ knots and $\geq 20$ knots respectively). Through the analysis in this report, the spatiotemporal overlap of the following factors favored mv-genesis within study QLCSs:

- Updraft towers 5 kilometers ahead to 5 kilometers behind the UDCZ
- $\geq 0$ knots of 0-1 km AGL and $\geq 20$ knots of 0-6 km AGL line-normal wind shear
- Rear-inflow surge causing a bow structure to leading convective line

Though this study uses a relatively large dataset of observed QLCS cases/events, tested for internal characteristics at relatively small intervals (i.e. 15 km), and used proximity soundings in close space/time to each QLCS, a few remaining caveats deserve additional discussion. The most important of these is the use of proximity sounding data to quantify the background

environment that may undergo rapid modification. Rapid storm-scale modifications represent a

challenge in accurately capturing the "true" environment using proximity sounding data. In

addition, strong mid and upper-level winds may introduce significant horizontal displacement of

certain soundings (and associated measures) from a study event of interest. As described in

Section 2.1, extra consideration was given at the onset of case selection to choose events in

which the associated proximity sounding has the greatest potential to represent the "true"

background atmosphere.

Another caveat, especially concerning analysis of thermodynamic variables, is an overall

limited sample size. This is especially true when comparing tornadic to non-tornadic MVs. Only

(9/42%) of MVs were tornadic during the period in which they were assessed. This makes

conclusions using this division of MVs preliminary in nature, and requires additional analysis

beyond this report.

Finally, to continue to build operational guidance for MV-gen identification and warning

strategies, future work should focus on increasing overall study QLCSs. As discussed in study

caveats, the overall case size (50) limits overall conclusivity of thermodynamic variable

outcomes. Composite sounding profiles, binned by case type (mv vs. non-mv), may also help

provide insight on favorable mv-genesis environments using an operationally valuable tool, and

will be developed beyond this report.

# References

Alfaro, D. A., 2017: Low-tropospheric shear in the structure of squall lines: Impacts on latent heating under layer-lifting ascent. *J. Atmos. Sci.*, **74**, 229–248, https://doi.org/10.1175/JAS-D-16-0168.1.

Alfaro, D. A., and Lezana, F., 2022: A momentum-balance theory for the updraft structure in density currents analogous to squall lines. Atmosfera.; **35**, https://doi.org/10.20937/ATM.52899

Anderson-Frey, A. K., Y. P. Richardson, A. R. Dean, R. L. Thompson, and B. T. Smith, 2016: Investigation of near-storm environments for tornado events and warnings. *Wea. Forecasting*, **31**, 1771–1790, https://doi.org/10.1175/WAF-D-16-0046.1.

Atkins, N. T., C. S. Bouchard, R. W. Przybylinski, R. J. Trapp, and G. Schmocker, 2005: Damaging surface wind mechanisms within the 10 June 2003 Saint Louis bow echo during BAMEX. *Mon. Wea. Rev.*, **133 ,** 2275–2296. https://doi.org/10.1175/MWR3100.1

Atkins, N. T., and M. St. Laurent, 2009a: Bow echo mesovortices. Part I: Processes that influence their damaging potential. *Mon. Wea. Rev.*, **137**, 1497–1513, https://doi.org/10.1175/2008MWR2649.1.

Atkins, N. T., and M. St. Laurent, 2009b: Bow echo mesovortices. Part II: Their genesis. *Mon. Wea. Rev.*, **137**, 1514–1532, https://doi.org/10.1175/2008MWR2650.1.

Brotzge, J., and S. E. Nelson, R. L. Thompson, and B. T. Smith, 2013: Tornado probability of detection and lead time as a function of convective mode and environmental parameters. Wea. Forecasting, **28**, 1261–1276, https://doi.org/10.1175/WAF-D-12-00119.1.

Bryan, G. H., D. Ahijevych, C. Davis, S. Trier, and M. Weisman, 2005: Observations of cold

pool properties in mesoscale convective systems during BAMEX. Preprints, *11th Conf.*

*on Mesoscale Processes,* Albuquerque, NM, Amer. Meteor. Soc., JP5J.12.

http://ams.confex.com/ams/pdfpapers/96718.pdf.

Bryan, G. H., and R. Rotunno, 2014: The optimal state for gravity currents in shear. *J. Atmos.*

*Sci.*, **71**, 448–468, https://doi.org/10.1175/JAS-D-13-0156.1

Carbone, R. E., 1983: A severe frontal rainband. Part II: Tornado parent vortex circulation. *J.*

*Atmos. Sci.*, 40, 2639–2654, https://doi.org/10.1175/1520-

0469(1983)040<2639:ASFRPI>2.0.CO;2.

Cohen, A. E., M. C. Coniglio, S. F. Corfidi, and S. J. Corfidi, 2007: Discrimination of mesoscale

convective system environments using sounding observations. Wea. Forecasting, **22**,

1045–1062, https://doi.org/10.1175/WAF1040.1.

Coniglio, M. C., D. J. Stensrud, and L. J. Wicker, 2006: Effects of upper-level shear on the

structure and maintenance of strong quasi-linear mesoscale convective systems. *J. Atmos.*

*Sci.,* 63, 1231–1252. https://doi.org/10.1175/JAS3681.1

Conrad, D. M., and K. R. Knupp, 2019: Doppler radar observations of horizontal shearing

instability in quasi-linear convective systems. *Mon. Wea. Rev.*, **147**, 1297–1318,

https://doi.org/10.1175/MWR-D-18-0257.1.

Flournoy, M. D., and M. C. Coniglio, 2019: Origins of vorticity in a simulated tornadic

mesovortex observed during PECAN on 6 July 2015. Mon. Wea. Rev., **147**, 107–134,

https://doi.org/ 10.1175/MWR-D-18-0221.1.

Fujita, T. T., 1978: Manual of downburst identification for project Nimrod. Satellite and

    Mesometeorology Research Paper 156, Dept. of Geophysical Sciences, University of

    Chicago, 104 pp. [NTIS PB-286048.]

Gibbs, J. G., and B. R. Bowers, 2019: Techniques and thresholds of significance for using WSR-

    88D velocity data to anticipate significant tornadoes. *J. Oper. Meteor.*, **7**, 117–137,

    https://doi.org/10.15191/NWAJOM.2019.0709.

Gibbs, J. G., 2021: Evaluating precursor signals for QLCS tornado and higher impact straight-

    line wind events. *J. Oper Meteor.*, **9 (5)**, 62-75,

    https://doi.org/10.15191/nwajom.2021.0905.

Haberlie, A. M., and W. S. Ashley, 2019: A radar-based climatology of mesoscale convective

    systems in the United States. *J. Climate*, **32**, 1591–1606, https://doi.org/10.1175/JCLI-D-

    18-0559.1.

Jorgensen, D. P., and B. F. Smull, 1993: Mesovortex circulations seen by airborne Doppler radar

    within a bow-echo mesoscale convective system. *Bull. Amer. Meteor. Soc.*, **74 ,** 2146–

    2157.

King, J. R., M. D. Parker, K. D. Sherburn, and G. M. Lackmann, 2017: Rapid evolution of cool

    season, low-CAPE severe thunderstorm environments. *Wea. Forecasting*, **32**, 763–778,

    https://doi.org/10.1175/WAF-D-16-0141.1.

Kirkpatrick, C., E. W. McCaul Jr., and C. Cohen, 2007: The motion of simulated convective

    storms as a function of basic environmental parameters. *Mon. Wea. Rev.*, **135**, 3033–

    3051. https://doi.org/10.1175/MWR3447.1

Lee, B. D., and R. B. Wilhelmson, 1997: The numerical simulation of non-supercell

    tornadogenesis. Part I: Initiation and evolution of pretornadic misocyclone circulations

    along a dry outflow boundary. *J. Atmos. Sci.*, **54**, 32–60, https://doi.org/10.1175/1520-

    0469(1997)054<0032:TNSONS>2.0.CO;2.

Mulholland, J. P., J. M. Peters, and H. Morrison, 2021: How does vertical wind shear influence

    entrainment in squall lines? *J. Atmos. Sci.*, **78**, 1931–1946, https://doi.org/10.1175/JAS-

    D-20-0299.1.

Parker, M. D., and R. H. Johnson, 2004a: Simulated convective lines with leading precipitation.

    Part I: Governing dynamics. *J. Atmos. Sci.*, **61**, 1637–1655, https://doi.org/10.1175/1520-

    0469(2004)061<1637:SCLWLP>2.0.CO;2.

Potvin, C. K., K. L. Elmore, and S. J. Weiss, 2010: Assessing the impacts of proximity sounding

    criteria on the climatology of significant tornado environments. *Wea. Forecasting*, **25 ,**

    921–930. https://doi.org/10.1175/2010WAF2222368.1

Przybylinski, R. W., 1995: The bow echo: Observations, numerical simulations, and severe

    weather detection methods. *Wea. Forecasting*, **10 ,** 203–218.

    https://doi.org/10.1175/1520-0434(1995)010<0203:TBEONS>2.0.CO;2

Rogers, J. W., B. A. Hagenhoff, A. E. Cohen, R. L Thompson, B. T. Smith, and E. E. Carpenter,

    2016: Lower Mississippi River Valley quasi-linear convective system tornado

    environments and radar signatures. *J. Operational Meteor*., **5** (4), 42-52,

    https://doi.org/10.15191/nwajom.2017.0504.

Rotunno, R., J. B. Klemp, and M. L. Weisman, 1988: A theory for strong, long-lived squall lines.

    *J. Atmos. Sci.*, **45**, 463–485, https://doi.org/10.1175/1520-

    0469(1988)045<0463:ATFSLL>2.0.CO;2.

Schaumann, J. S., and R. W. Przybylinski, 2012: Operational application of 0–3 km bulk shear

　　vectors in assessing quasi linear convective system mesovortex and tornado potential.

　　*26th Conf. on Severe Local Storms*, Nashville, TN, Amer. Meteor. Soc., 142,

　　https://ams.confex.com/ams/26SLS/webprogram/Paper212008.html.

Schenkman, A. D., M. Xue, and A. Shapiro, 2012: Tornadogenesis in a simulated mesovortex

　　within a mesoscale convective system. *J. Atmos. Sci.*, **69**, 3372–3390,

　　https://doi.org/10.1175/JAS-D-12-038.1.

Sessa, M. F., and R. J. Trapp, 2020: Observed relationship between tornado intensity and

　　pretornadic mesocyclone characteristics. *Wea. Forecasting*, **35**, 1243–1261,

　　https://doi.org/10.1175/WAF-D-19-0099.1.

Sherburn, K. D., and M. D. Parker, 2014: Climatology and ingredients of significant severe

　　convection in high-shear, lowCAPE environments. Wea. Forecasting, **29**, 854–877,

　　https:// doi.org/10.1175/WAF-D-13-00041.1.

Smith, B. T., R. L. Thompson, J. S. Grams, C. Broyles, and H. E. Brooks, 2012: Convective

　　modes for significant severe thunderstorms in the contiguous United States. Part I: Storm

　　classification and climatology. *Wea. Forecasting*, **27**, 1114–1135,

　　https://doi.org/10.1175/WAF-D-11-00115.1.

Smith, B. T., R. L. Thompson, A. R. Dean, and P. T. Marsh, 2015: Diagnosing the conditional

　　probability of tornado damage rating using environmental and radar attributes. *Wea.*

　　*Forecasting*, 30, 914–932, https://doi.org/10.1175/WAF-D-14-00122.1.

Thompson, R. L., R. Edwards, J. A. Hart, K. L. Elmore, and P. Markowski, 2003: Close

　　proximity soundings within supercell environments obtained from the Rapid Update

Cycle. *Wea. Forecasting*, **18**, 1243–1261, https://doi.org/10.1175/1520-0434(2003)018<1243:CPSWSE>2.0.CO;2.

Thompson, R. L., B. T. Smith, J. S. Grams, A. R. Dean, and C. Broyles, 2012: Convective modes for significant severe thunderstorms in the contiguous United States. Part II: Supercell and QLCS tornado environments. *Wea. Forecasting*, **27**, 1136–1154, https://doi.org/10.1175/WAF-D-11-00116.1.

Trapp, R. J., and M. L. Weisman, 2003: Low-level mesovortices within squall lines and bow echoes. Part II: Their genesis and implications. *Mon. Wea. Rev.*, **131**, 2804–2823, https://doi.org/10.1175/1520-0493(2003)131<2804:LMWSLA>2.0.CO;2.

Trapp, R. J., S. A. Tessendorf, E. S. Godfrey, and H. E. Brooks, 2005b: Tornadoes from squall lines and bow echoes. Part I: Climatological distribution. *Wea. Forecasting*, **20**, 23–34, https://doi.org/10.1175/WAF-835.1.

Wakimoto, R. M., H. V. Murphey, C. A. Davis, and N. T. Atkins, 2006b: High winds generated by bow echoes. Part II: The relationship between the mesovortices and damaging straight-line winds. *Mon. Wea. Rev.*, **134**, 2813–2829, https://doi.org/10.1175/MWR3216.1.

Weisman, M. L., and R. Rotunno, 2004: "A theory for strong, long-lived squall lines" revisited. *J. Atmos. Sci.*, **61**, 361–382. https://doi.org/10.1175/1520-0469(2004)061<0361:ATFSLS>2.0.CO;2

Wheatley, D. M., R. J. Trapp, and N. T. Atkins, 2006: Radar and damage analysis of severe bow echoes observed during BAMEX. *Mon. Wea. Rev.*, **134 ,** 791–806. https://doi.org/10.1175/MWR3100.1

Wheatley, D. M., and R. J. Trapp, 2008: The effect of mesoscale heterogeneity on the genesis

and structure of mesovortices within quasi-linear convective systems. *Mon. Wea. Rev.*,

136, 4220–4241, https://doi.org/10.1175/2008MWR2294.1.

Xu, X., M. Xue, and Y. Wang, 2015: The genesis of mesovortices within a real-data simulation

of a bow echo system. *J. Atmos. Sci.*, **72**, 1963–1986, https://doi.org/10.1175/JAS-D-14-

0209.1.
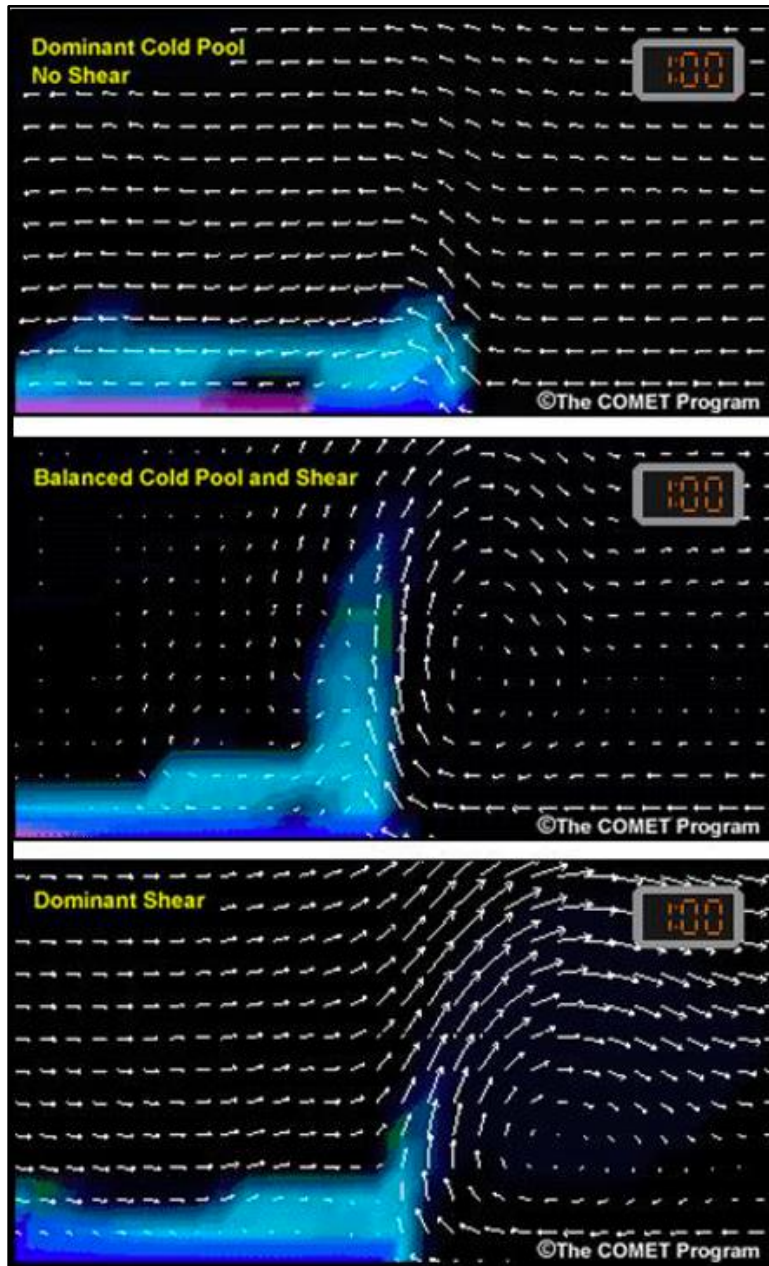
**Figure 1.** Overview of simulations depicting three shear cold/pool balance regimes in an x-z plane. White arrows represent two-dimensional air parcel motions. Blue and purple shading represent the system cold pool. Figure adapted from COMET modules of Weisman and Przybylinski (1999).
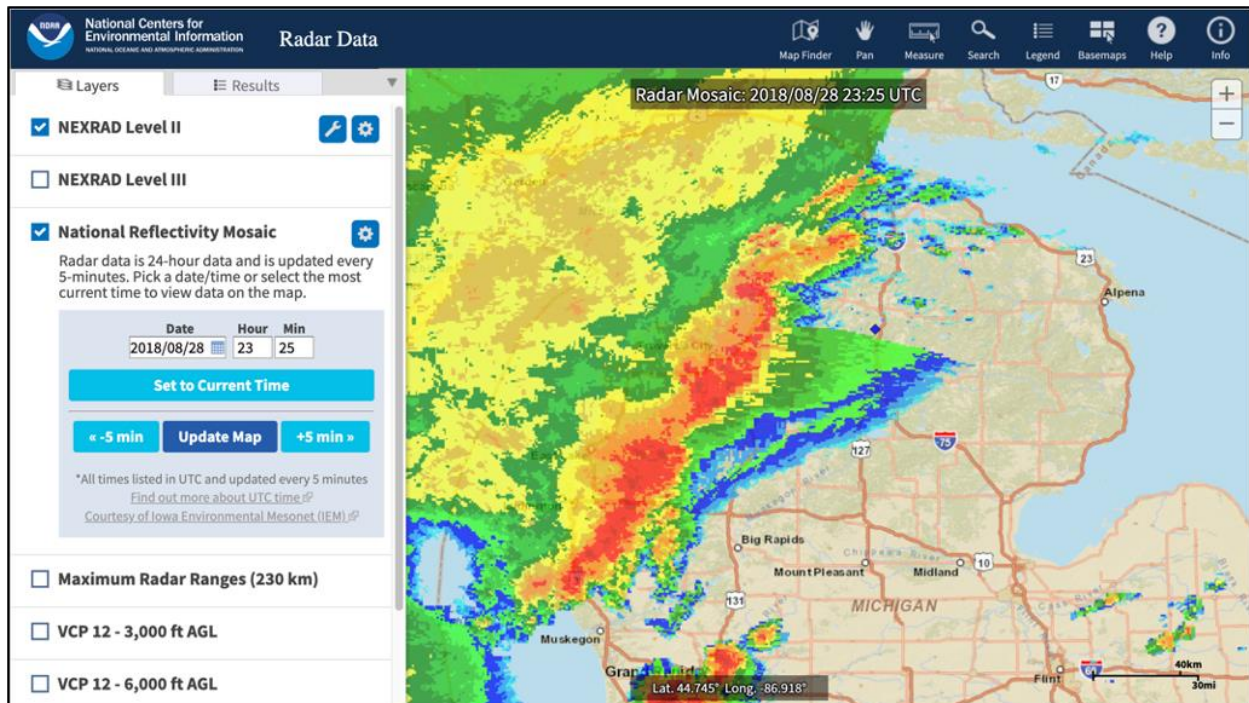
**Figure 2.** Example output from National Centers for Environmental Information (NCEI) interactive composite radar tool. Composite radar image at 2325 UTC from a study case across northern Michigan on 28 August 2018.
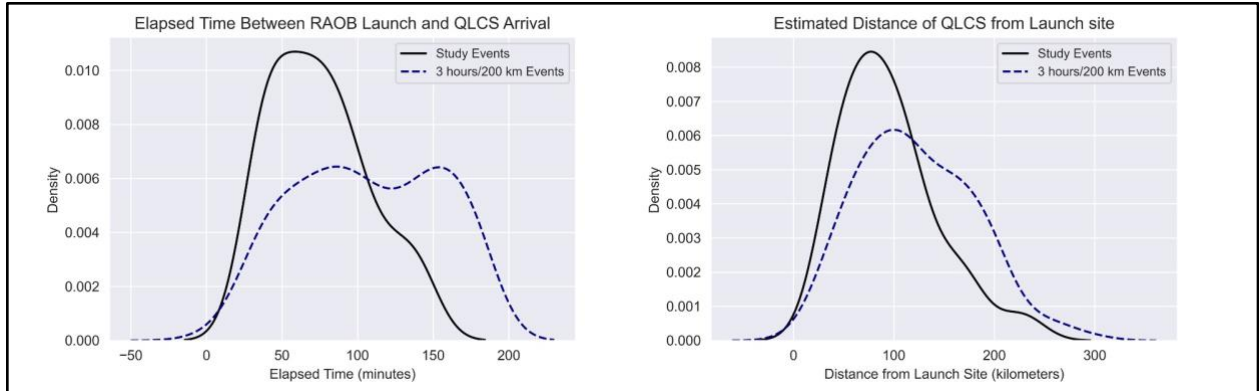
**Figure 3.** (Left panel) Kernel Density Estimation (KDE) plot of elapsed time after launch between 50 selected study events (black) and cases that passed intermediate threshold (dashed blue). (Right panel) KDE plot of QLCS distance at launch time between 50 selected study events (black) and cases that passed the intermediate threshold (dashed blue).
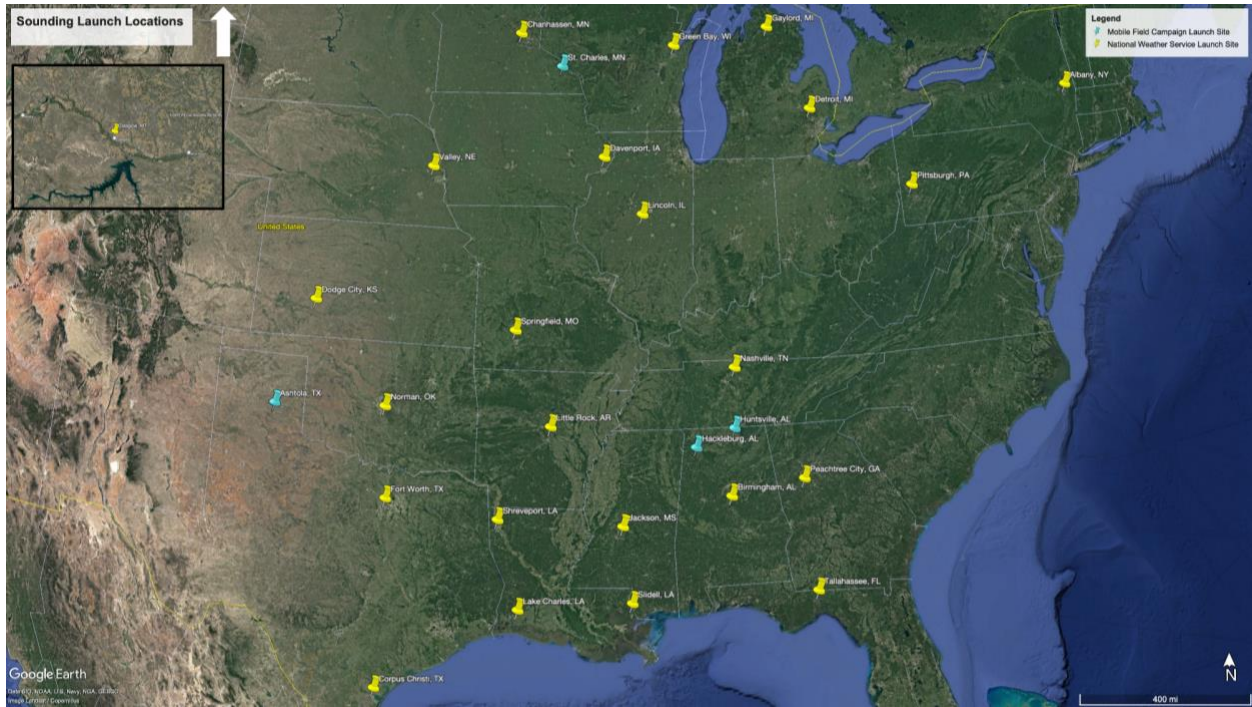
**Figure 4.** Geographical overview of proximity sounding launch sites. Inset represents Glasgow, MT National Weather Service launch location. Imagery courtesy of Google Earth.
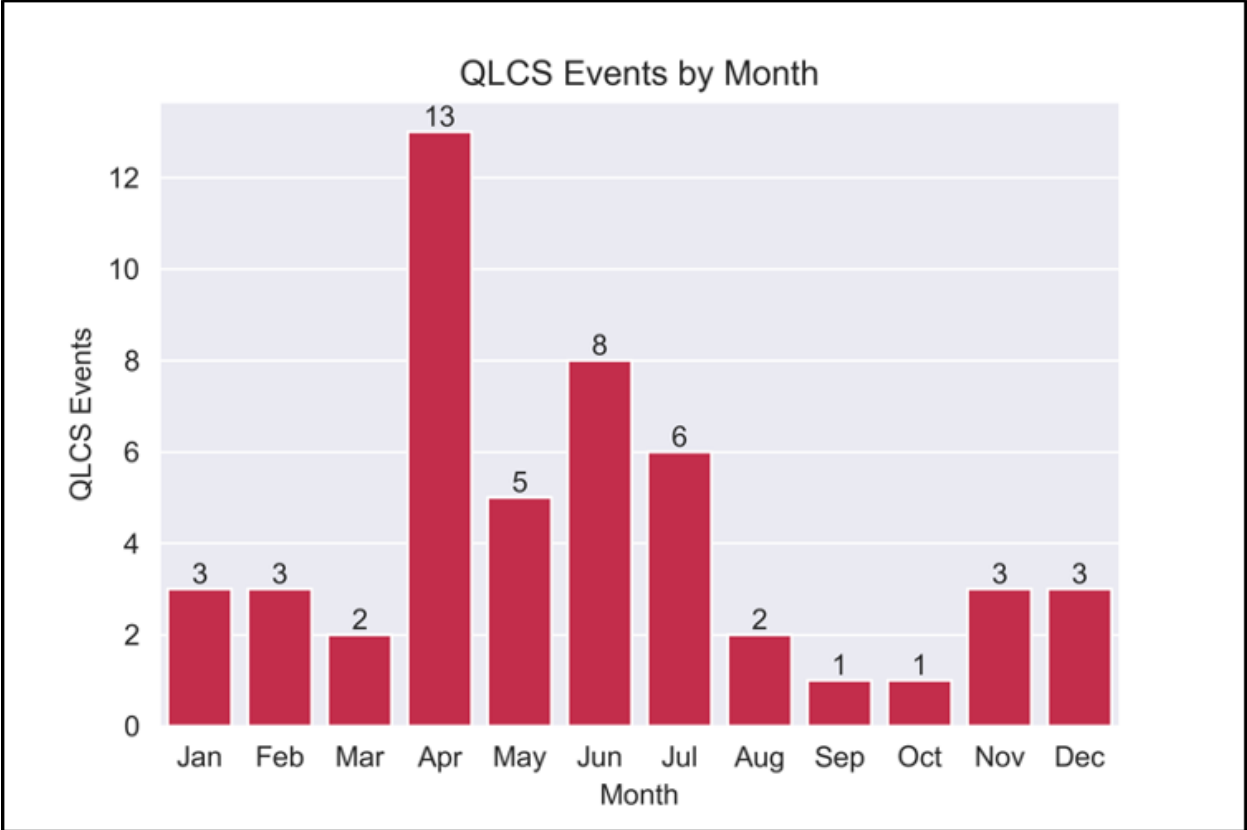
**Figure 5.** Bar graph plot showing distribution of 50 study QLCS cases by month.
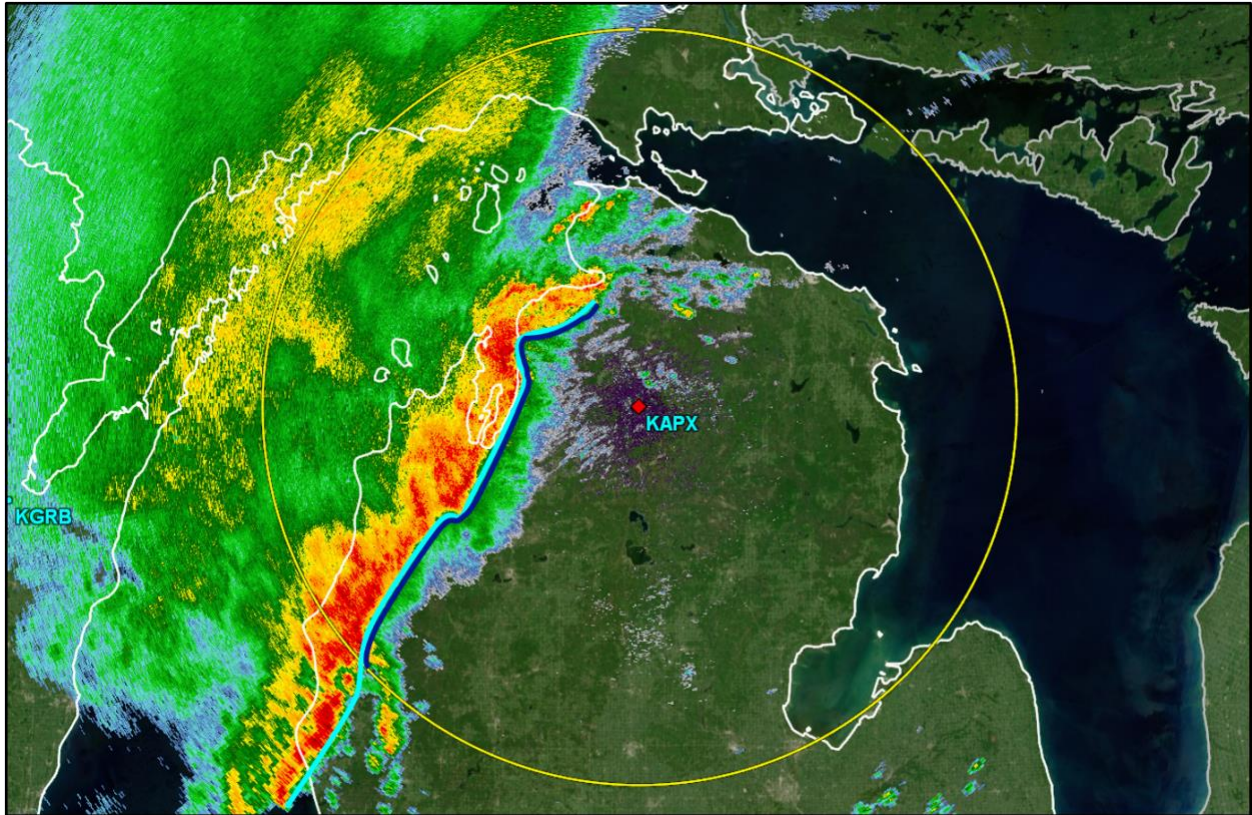
**Figure 6.** Overview of conditions defined for radar analysis in Section 2.2. 0.5° radar reflectivity image at 2316 UTC from KAPX WSR-88D radar. From observed QLCS on 28 August 2018 across northern Michigan. Yellow ring represents the 100 km radial from KAPX. Cyan line represents a portion of QLCS meeting Haberlie and Ashley (2019) definition. Dark blue line represents the portion of QLCS available for analysis.
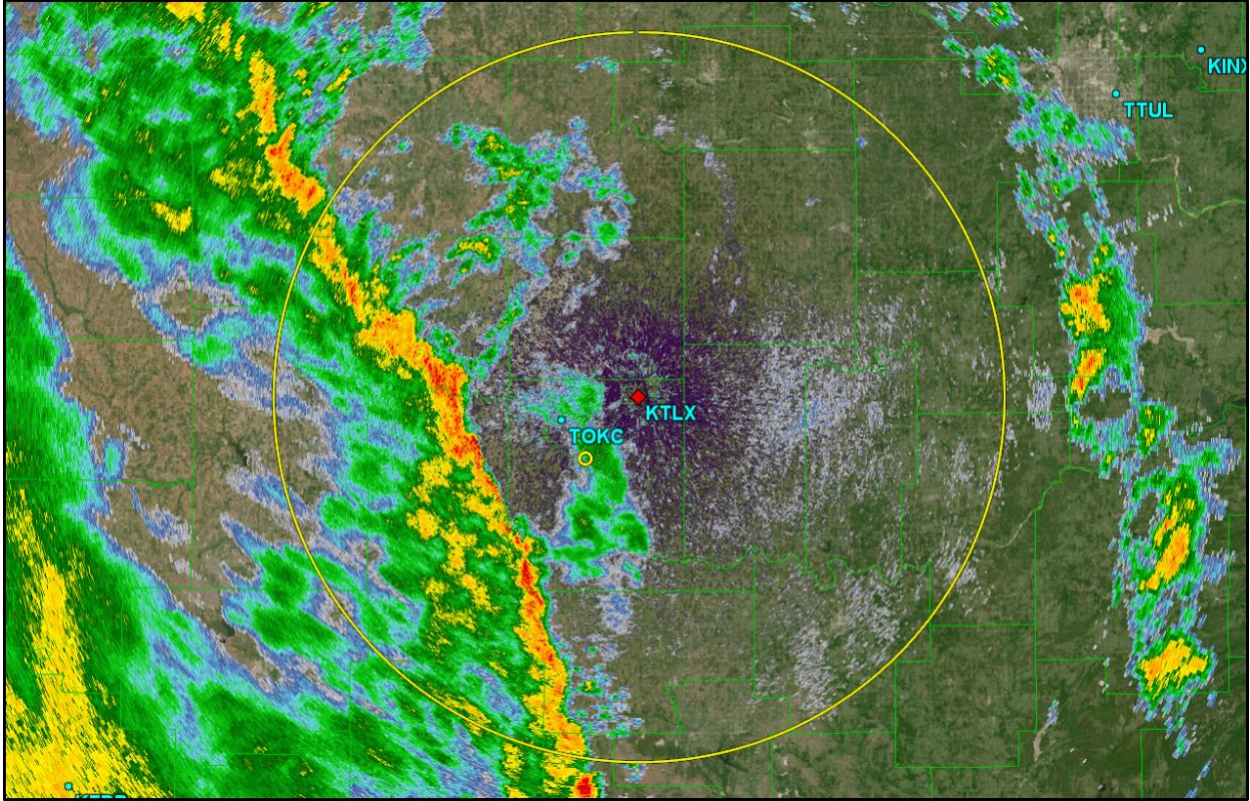
**Figure 7.** Example of "mismatched" QLCS case from 9 October 2018. 0.5° radar reflectivity image at 1125 UTC from KTLX WSR-88D radar. Yellow ring represents the 100 km radial from KTLX. Smaller yellow ring (radius of 2 km) represents the location of National Weather Service Norman, OK launch location.
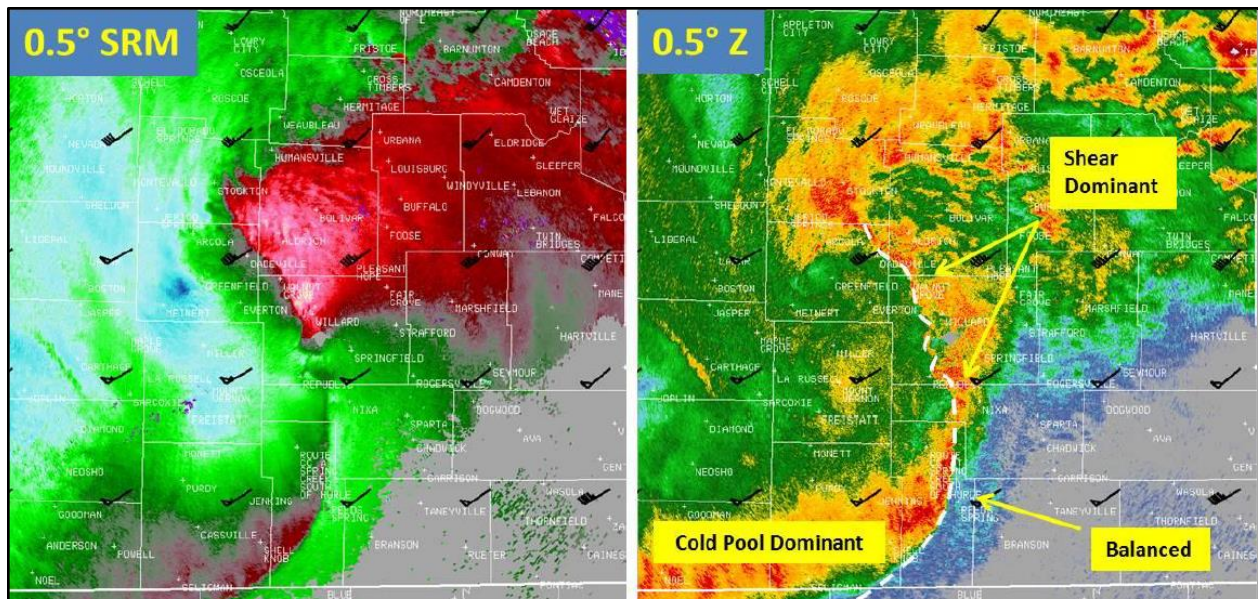
**Figure 8.** 0.5° storm-relative motion (SRM, left) and reflectivity (Z, right) from the KSGF WSR-88D radar at 1307 UTC on 8 May 2009. Comparison of updraft-downdraft convergence zone (dashed white line in right panel) to 0.5° Z highlights three different shear/cold pool balance regimes present at 1307 UTC. Black arrows represent 0-3 km bulk shear wind vectors derived from Rapid Refresh numerical model output. Figure adapted from Schaumann and Przybylinski (2012).
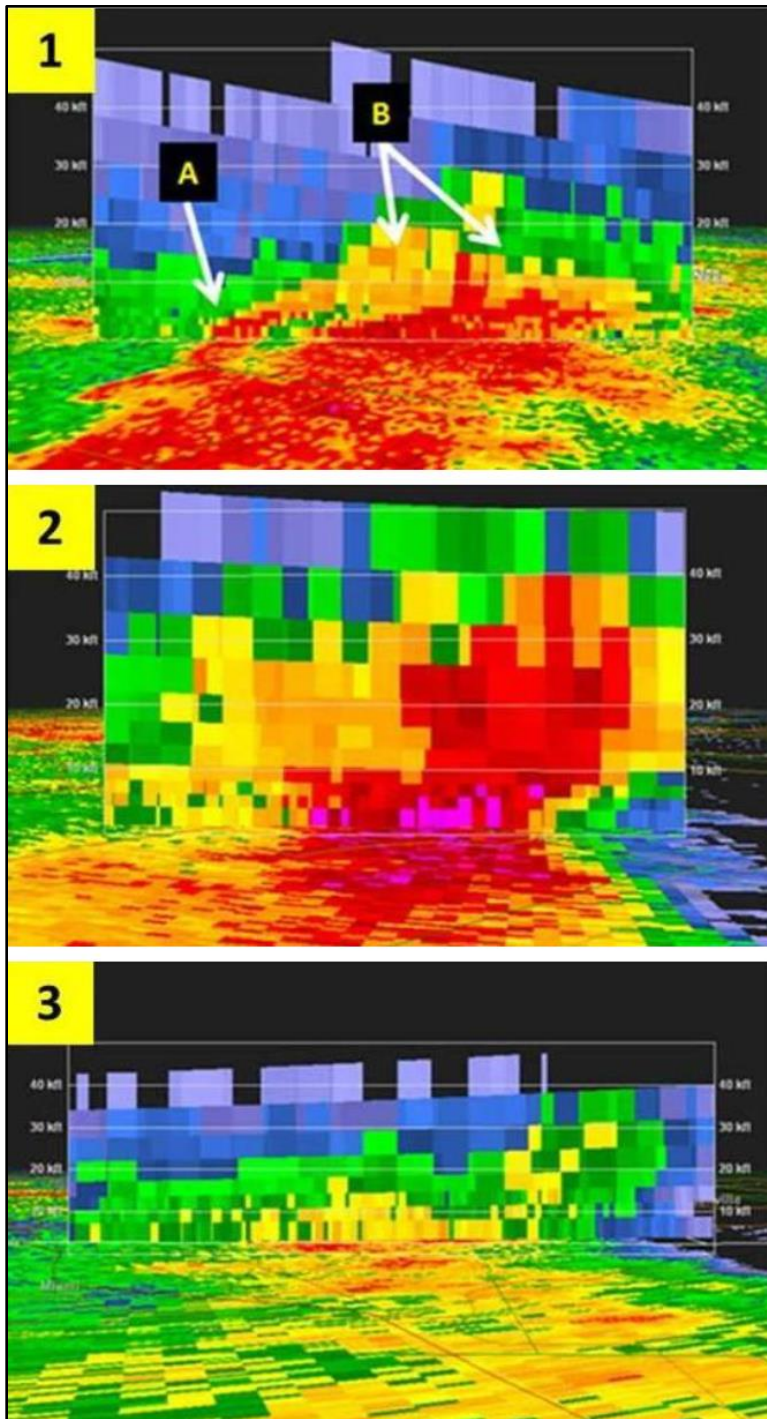
**Figure 9.** Reflectivity cross-sections (in x-z plane) from KSGF radar at 1307 UTC on 8 May 2009. All three panels are concurrent images depicting three different shear/cold pool balance regimes present at that time. 'A' and 'B' arrows on panel #1 (top) captures two shear/cool pool balance regimes ('balanced' and 'slightly shear dominant') in close proximity at 1307 UTC. Images courtesy of Gibson Ridge Analyst2 output, with the figure adapted from Schaumann and Przybylinski (2012).
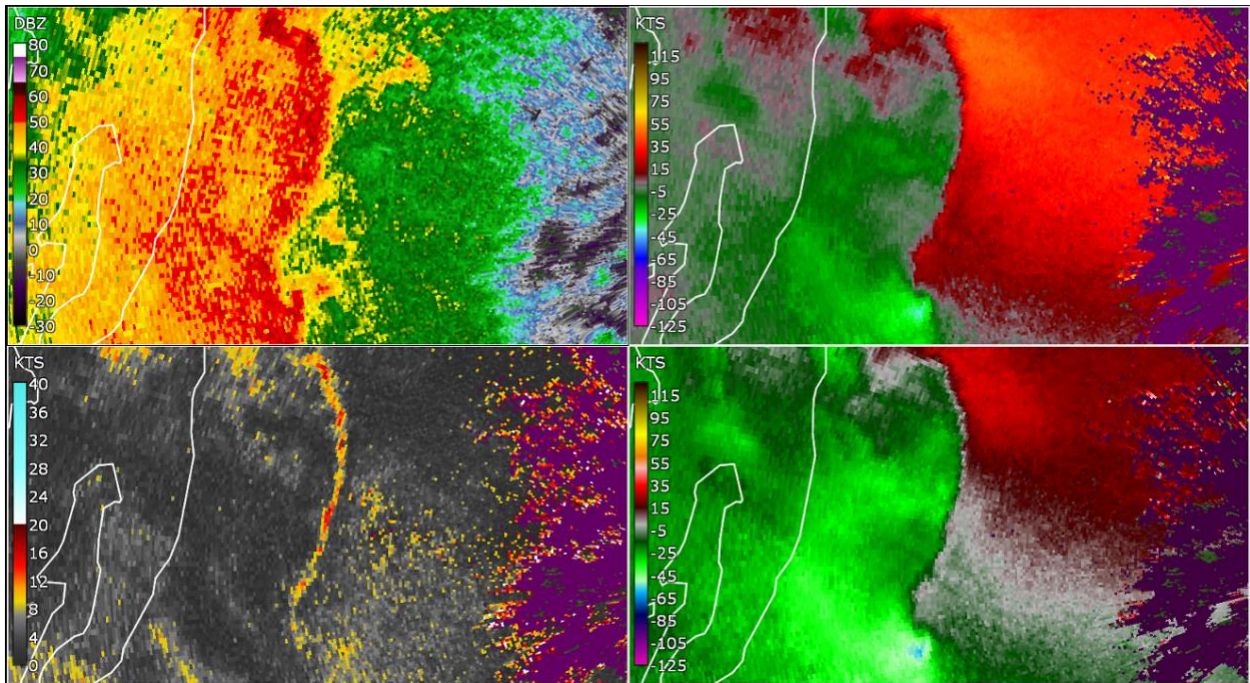
**Figure 10.** 4-panel visualization in Gibson Ridge 2 Analyst (GR2Analyst) setup for assessing U-to-R distance (i.e. shear/cold pool balance). From top right (and moving clockwise): radar reflectivity (Z), storm relative velocity/motion (SRV/M), base velocity (BV), spectrum width (SW). Image at 1604 UTC (from KAPX radar) on 28 August 2018.
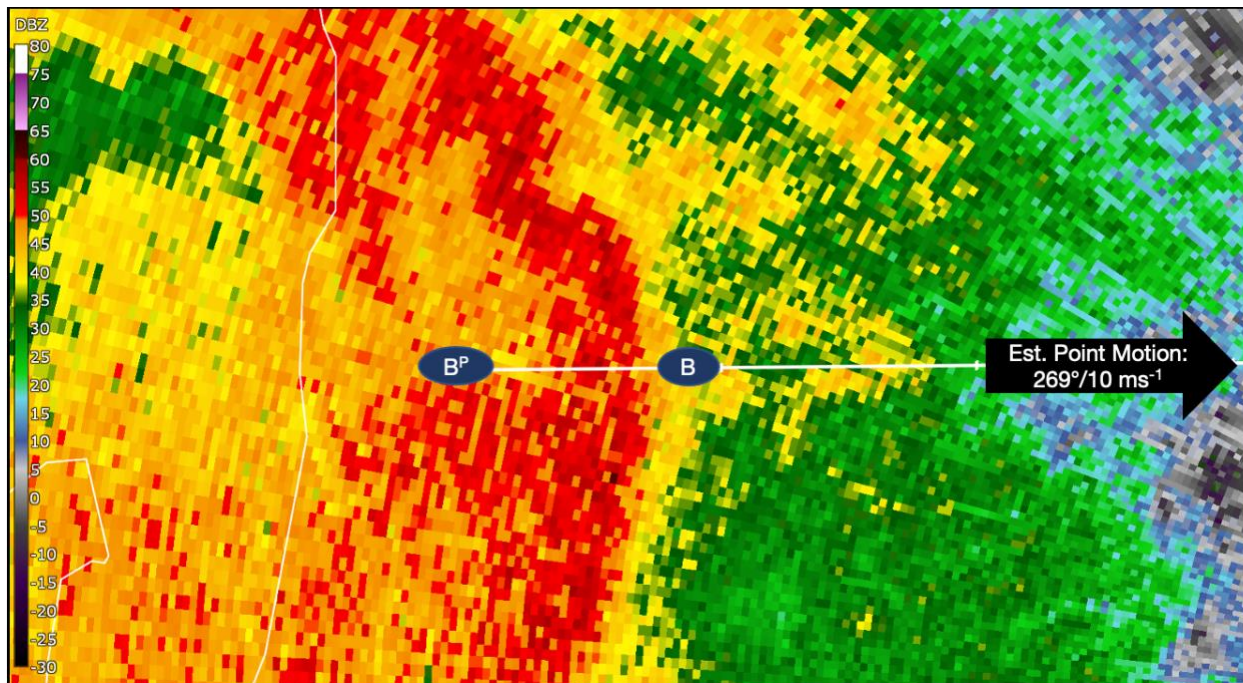
**Figure 11**. Portion of QLCS from 28 August 2018 event. Image at 2316 UTC from KAPX radar. Point 'B^P' represents position of point 'B' at prior analysis period (i.e. full volume scan).
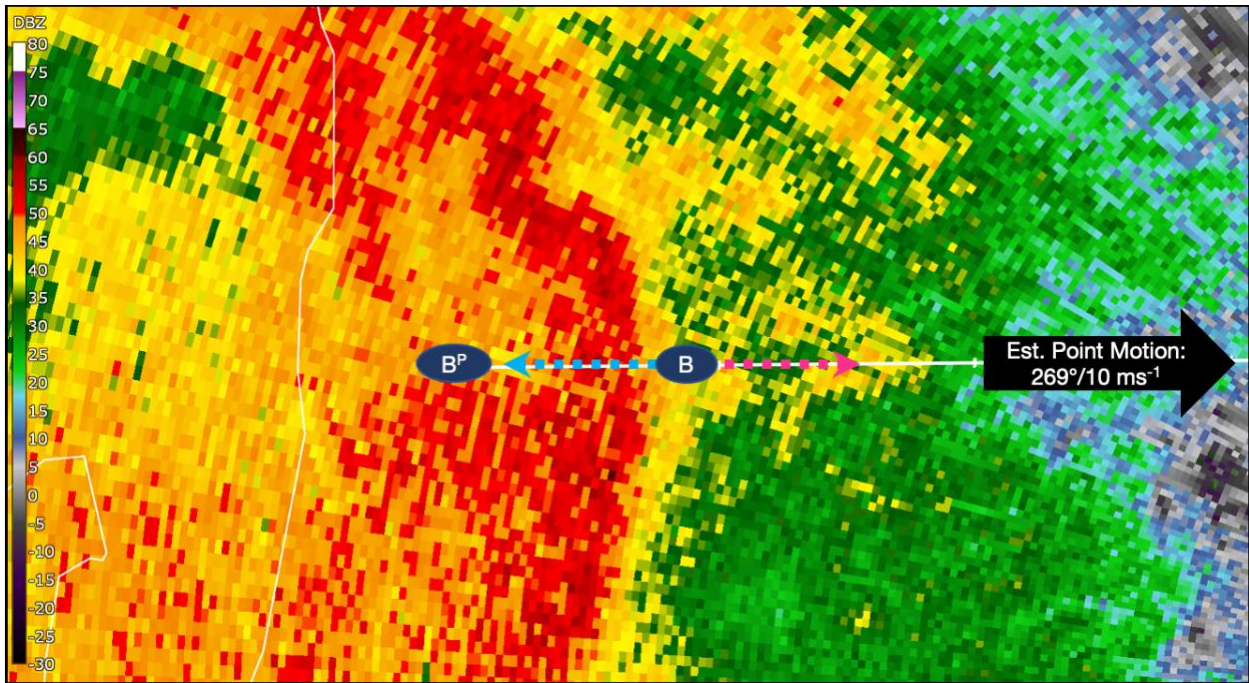
**Figure 12.** As in Fig. 11. Blue arrow corresponds to a negative (-) U-to-R distance. Pink arrow represents a positive (+) U-to-R distance.
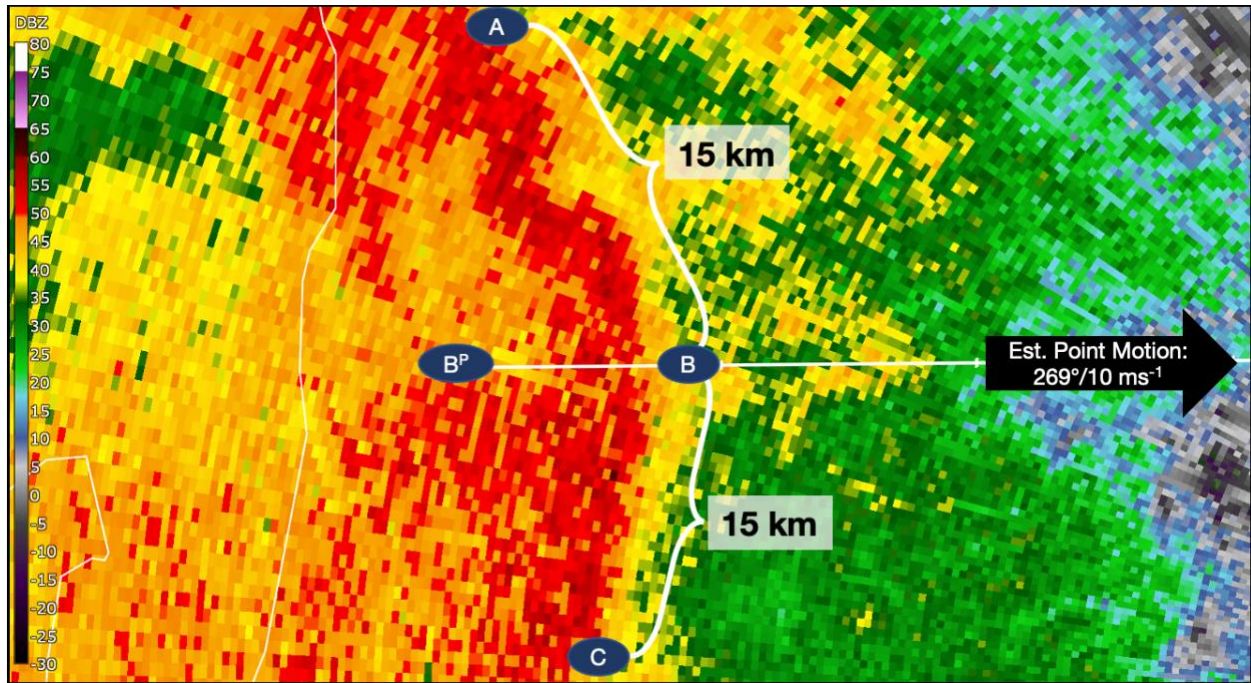
**Figure 13.** As in Fig. 11. Points 'A' and 'C' represent additional analysis points along the convective line (at 15 km intervals).
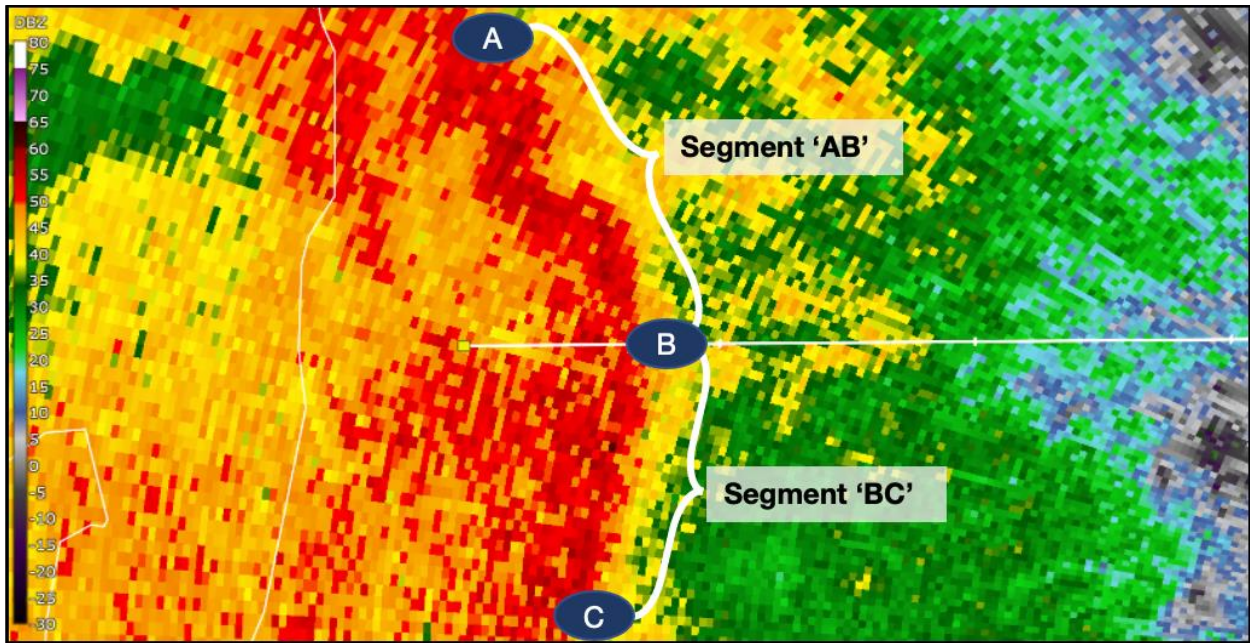
**Figure 14.** As in Fig. 11. Example of process to create analysis segments, where points 'A', 'B', and 'C' are the same as in Fig. 13.
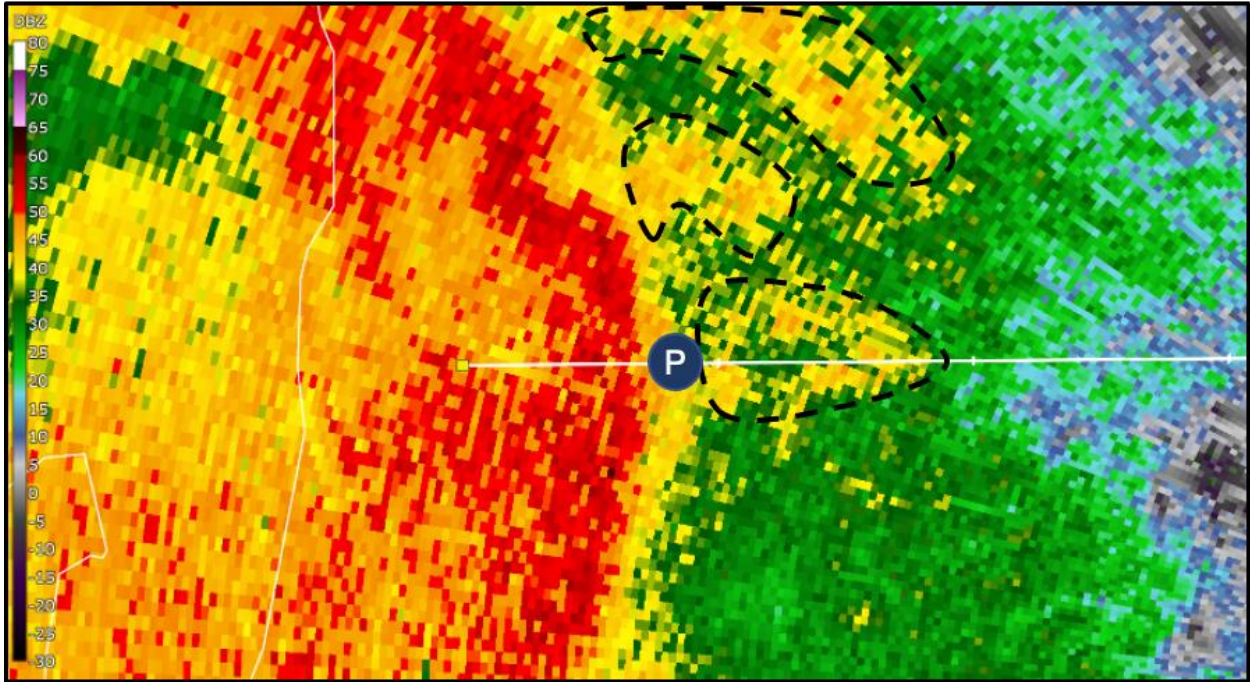
**Figure 15.** As in Fig. 11. Point 'P' same as point 'B' in Figs. 11-14. Black outlined regions correspond to radar artifact termed "enhanced reflectivity".
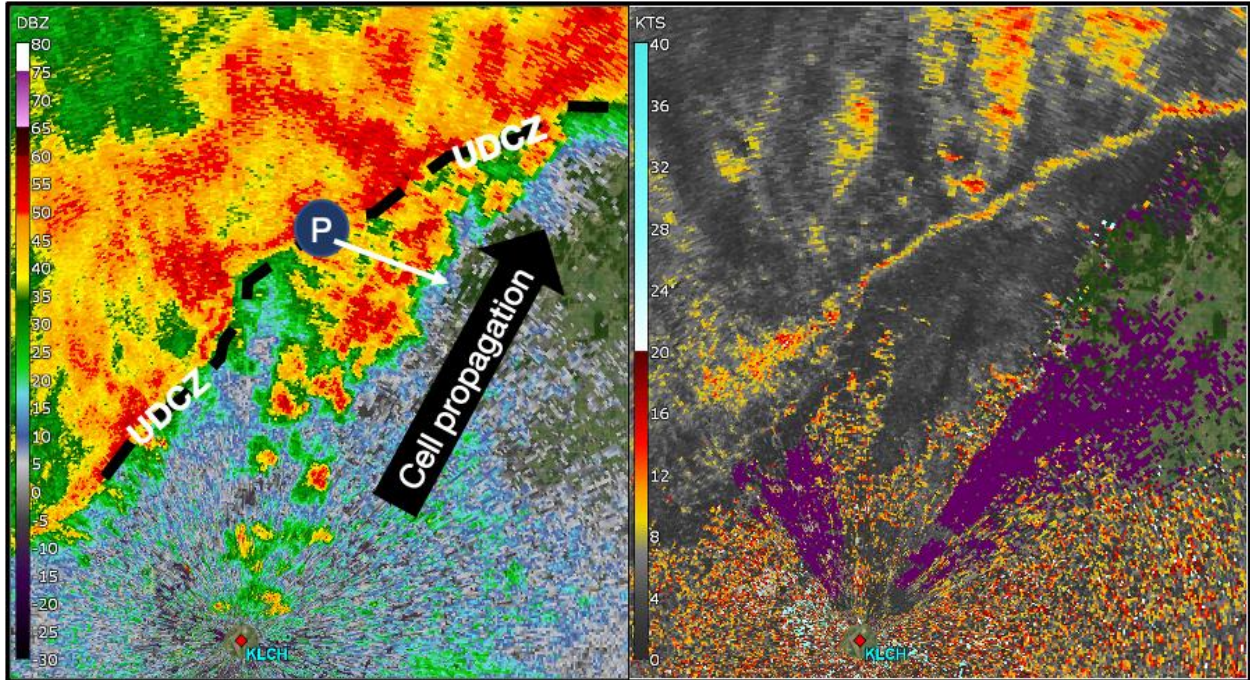
**Figure 16.** Study QLCS across southwestern Louisiana. Image representative of 1130 UTC volume scan from KLCH radar. Radar reflectivity (left panel) and spectrum width (right panel) shown. Dashed black line represents the identified position of UDCZ. Point 'P' represents a plausible analysis location.
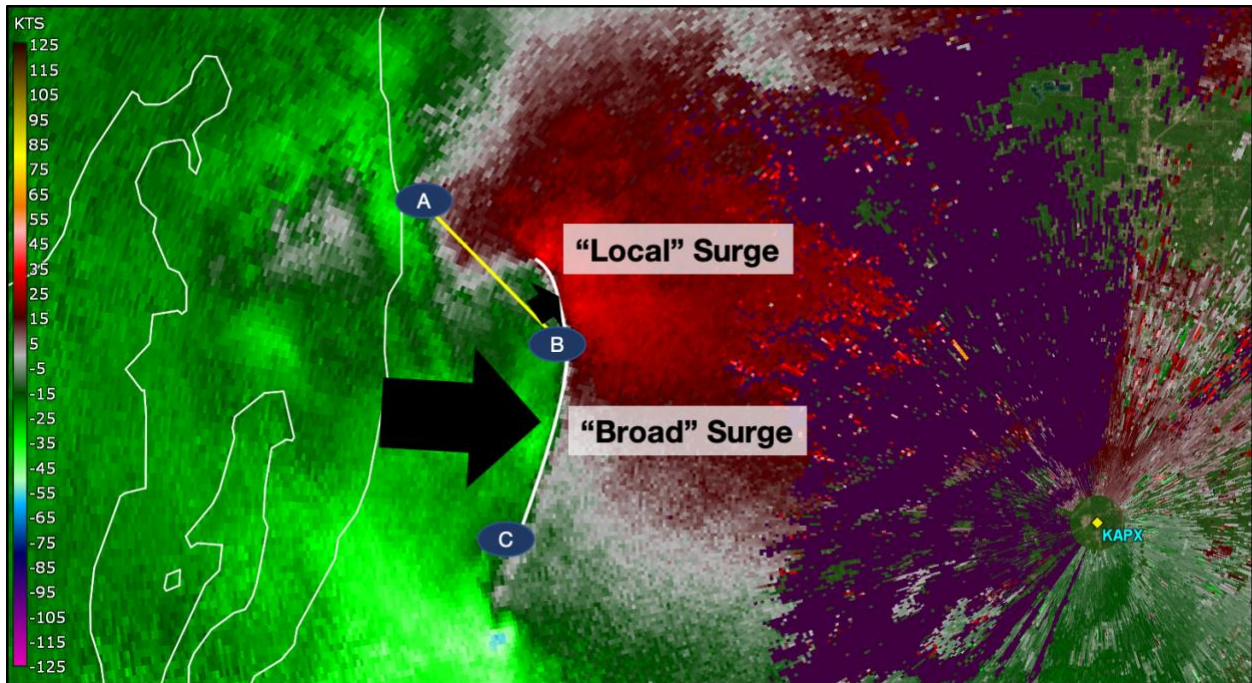
**Figure 17.** Example of process to determine rear-inflow surges (both "local" and "broad"). Base velocity (BV) image from 2316 UTC at KAPX radar. Positions 'A', 'B', and 'C' represent U-to-R analysis positions. Yellow line represents the 'AB' line segment. White line represents the leading edge of the "broad" rear-inflow surge. Black arrow represents the core of the rear-to-front flow at 2316 UTC.
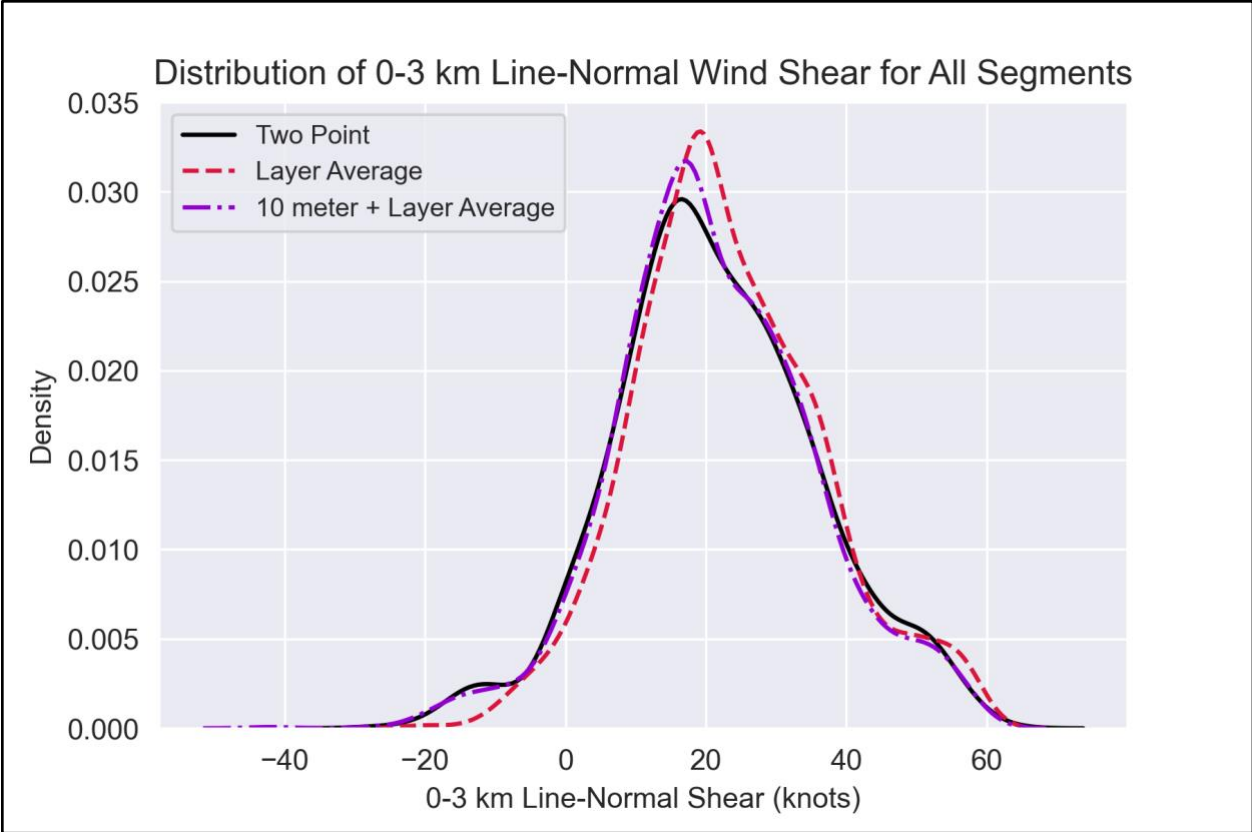
**Figure 18.** Kernel Density Estimation distribution comparing three different wind shear calculation approaches.
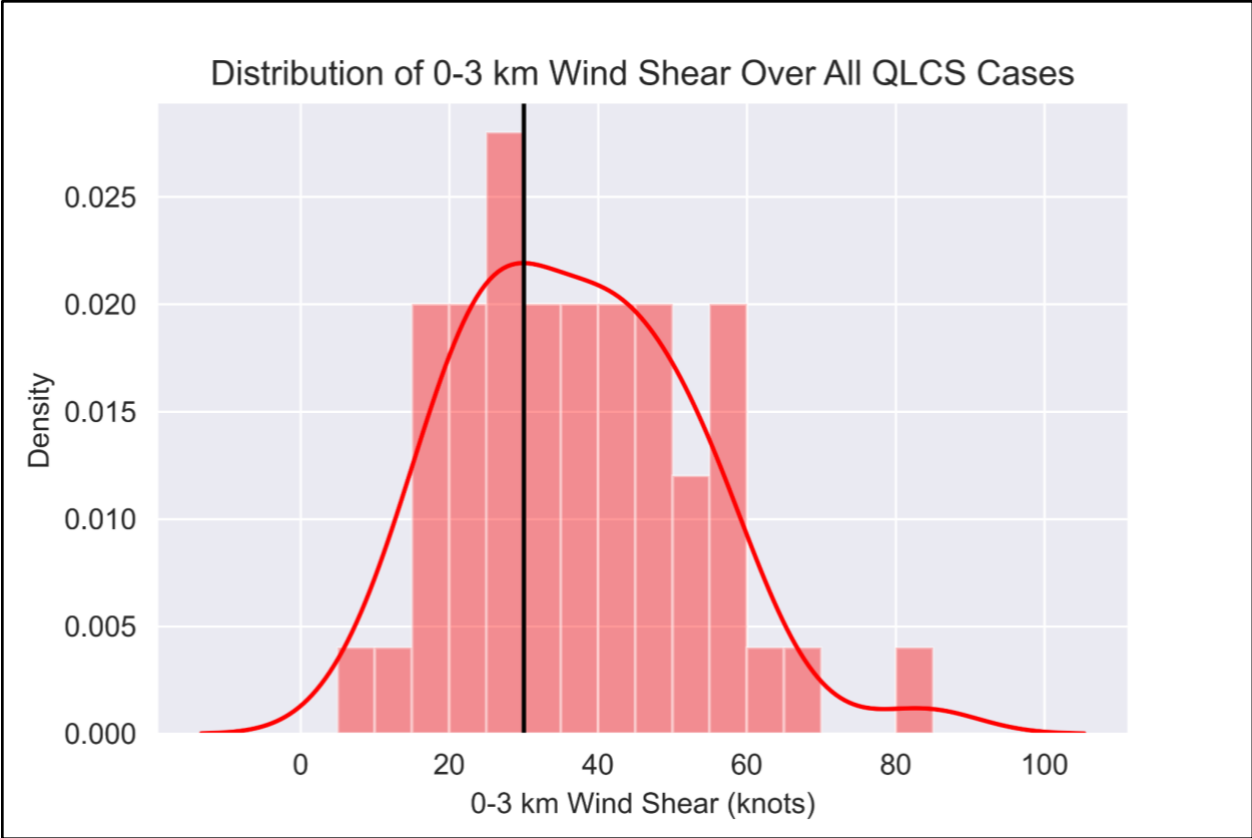
**Figure 19.** Kernel Density Estimation distribution of environmental 0-3 km bulk wind shear calculated from the proximity sounding associated with each study QLCS case. Vertical black line delineates the 30 kt threshold of the 3-I-M.
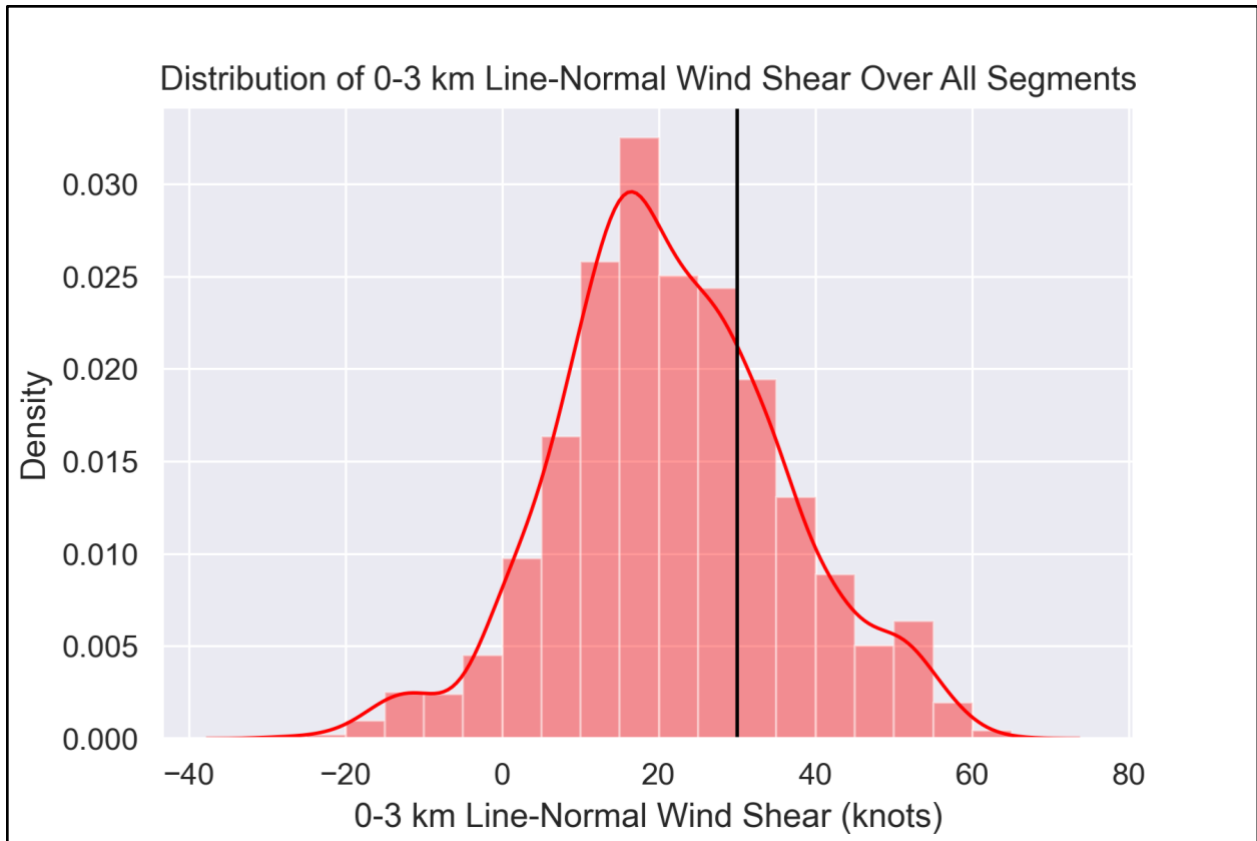
**Figure 20.** Kernel Density Estimation distribution of line-normal 0-3 km bulk wind shear calculated across each analysis segment for all QLCS events. Vertical black line delineates the 30 kt threshold of the 3-I-M.
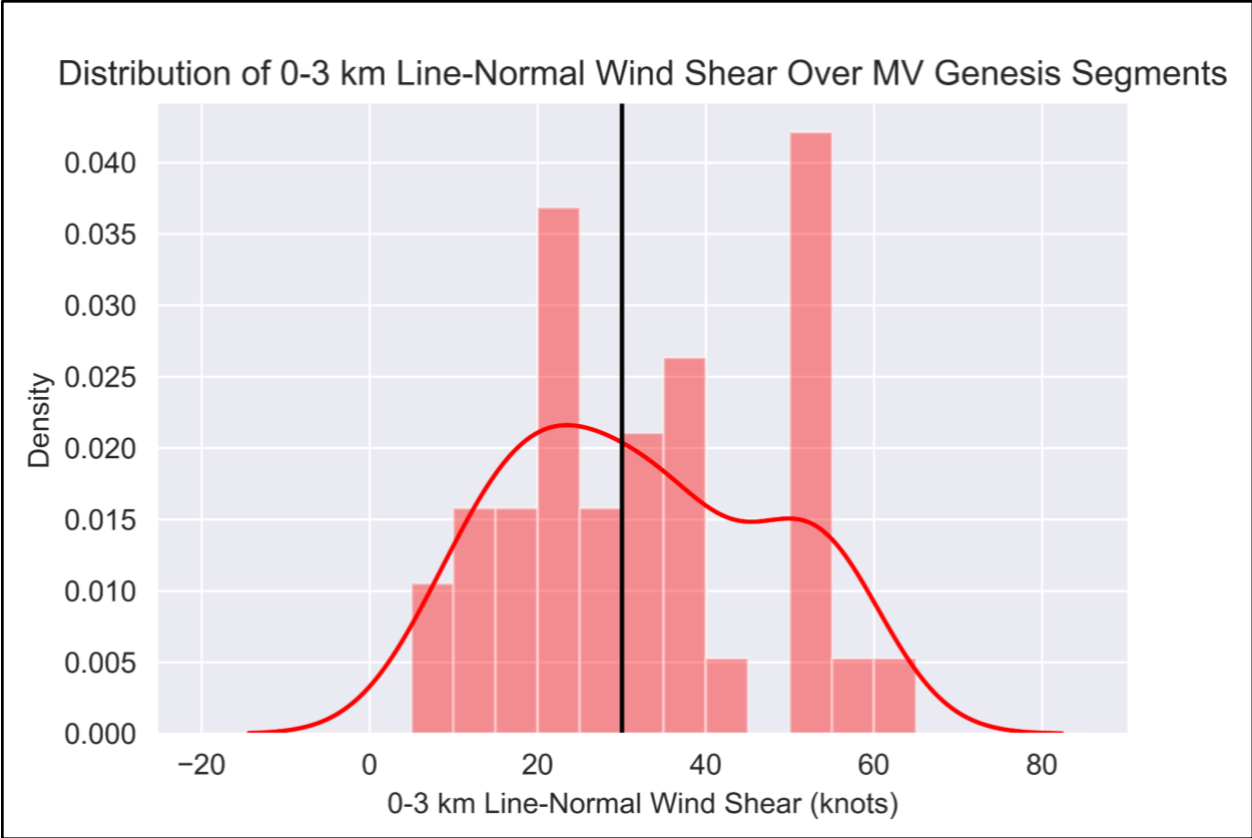
**Figure 21.** Kernel Density Estimation distribution of line-normal 0-3 km bulk wind shear calculated across each line segment where mv-genesis was assessed. Vertical black line delineates the 30 kt threshold of the 3-I-M.
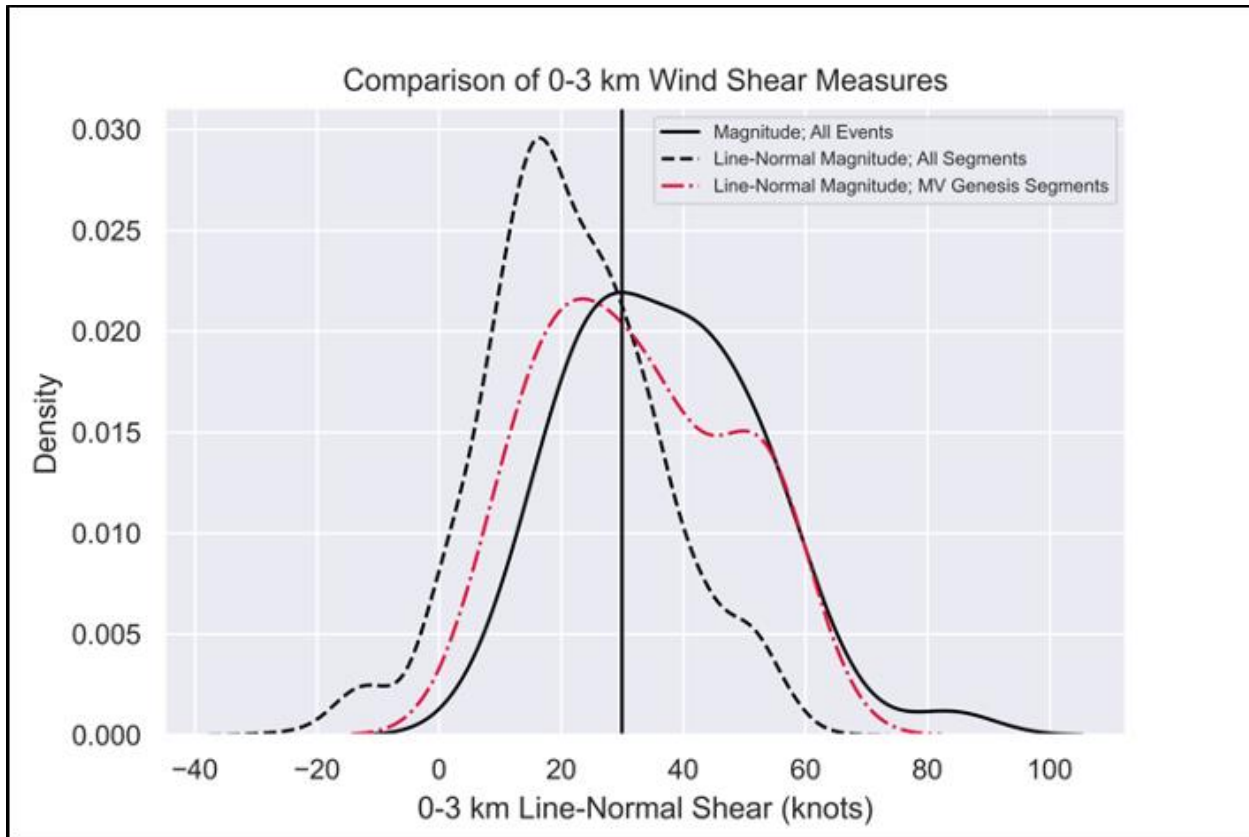
**Figure 22.** Kernel Density Estimation distribution comparison of 0-3 km bulk shear across all events and in line-normal components. Vertical black line delineates the 30 kt threshold of the 3-I-M.
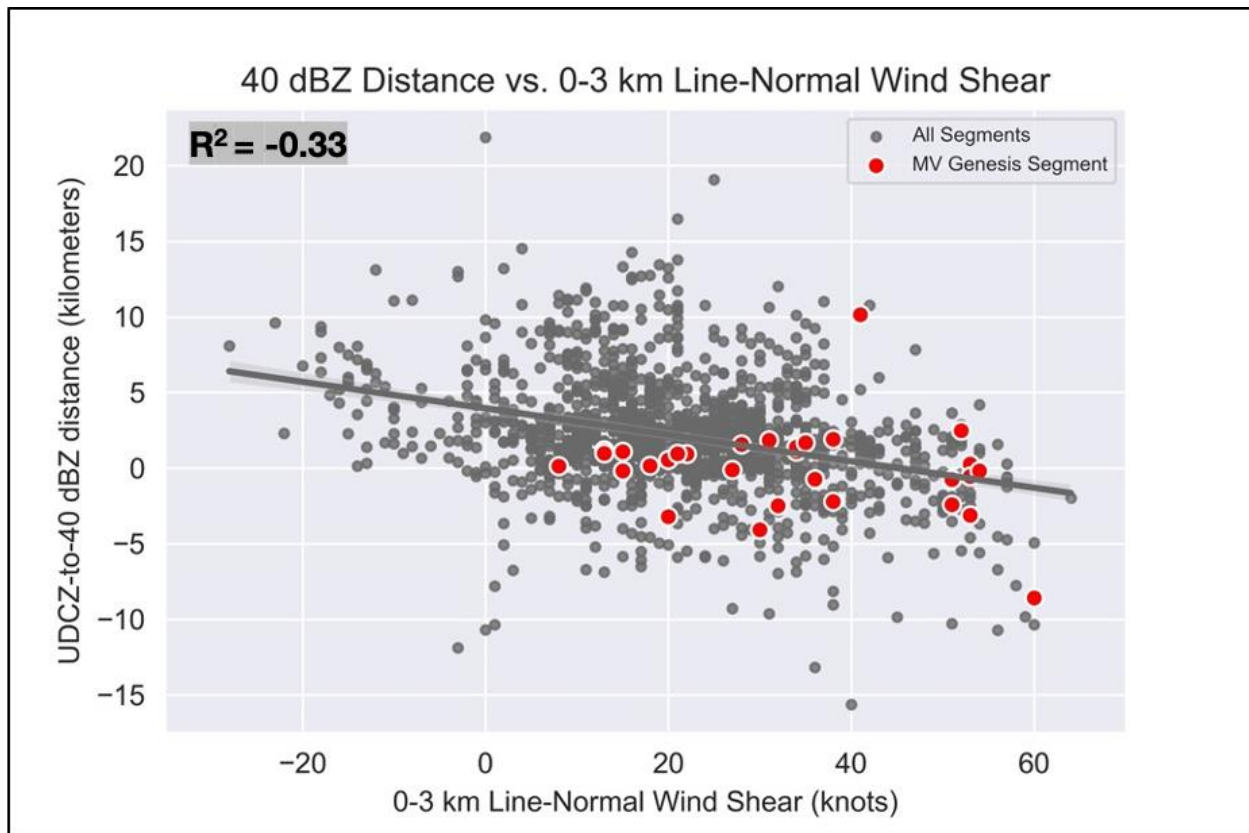
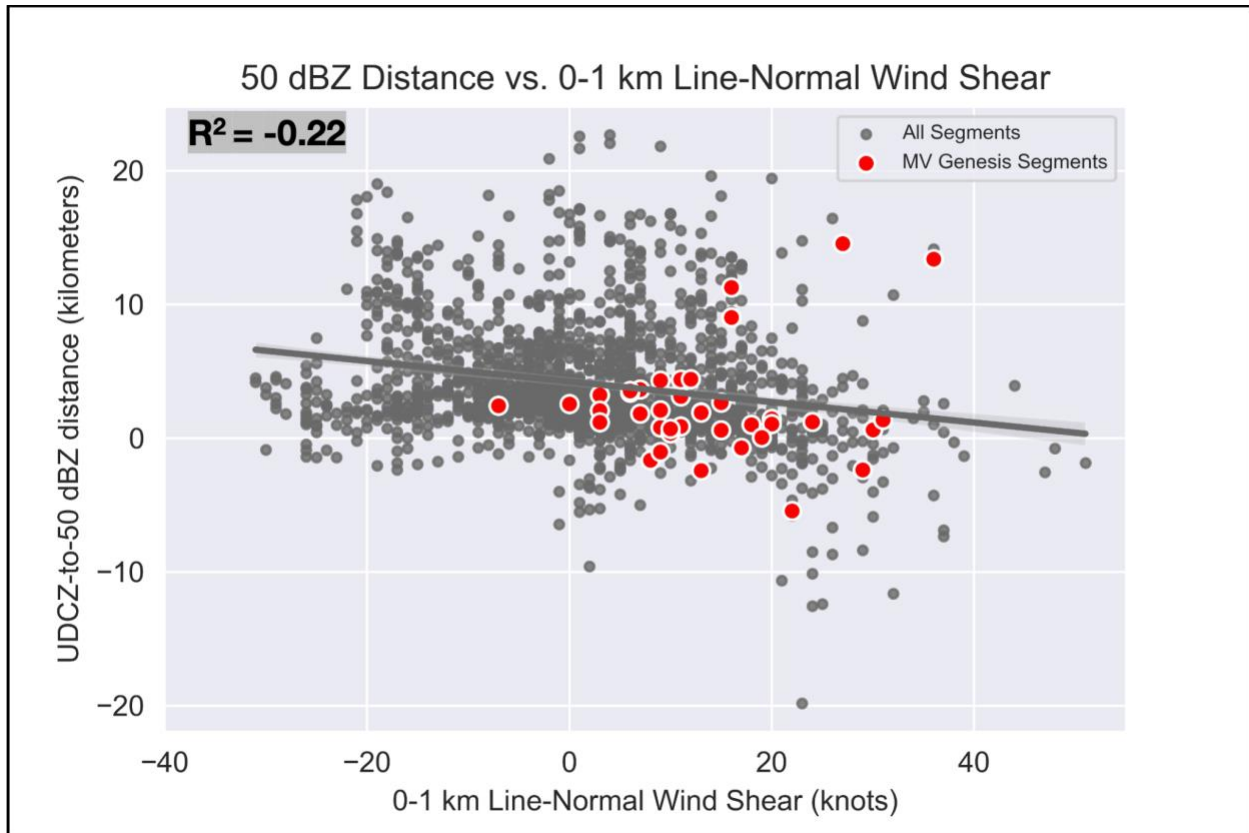**Figure 23.** Scatterplot comparing the shear/cold balance and wind shear 3-I-M ingredients using the 40 dBZ reflectivity threshold. Linear regression line represented as gray line (95% confidence interval shown as light gray shading), with Pearson correlation coefficient value ($R^2$) displayed in the top left corner. Red scatters represent segments where mv-genesis was assessed.
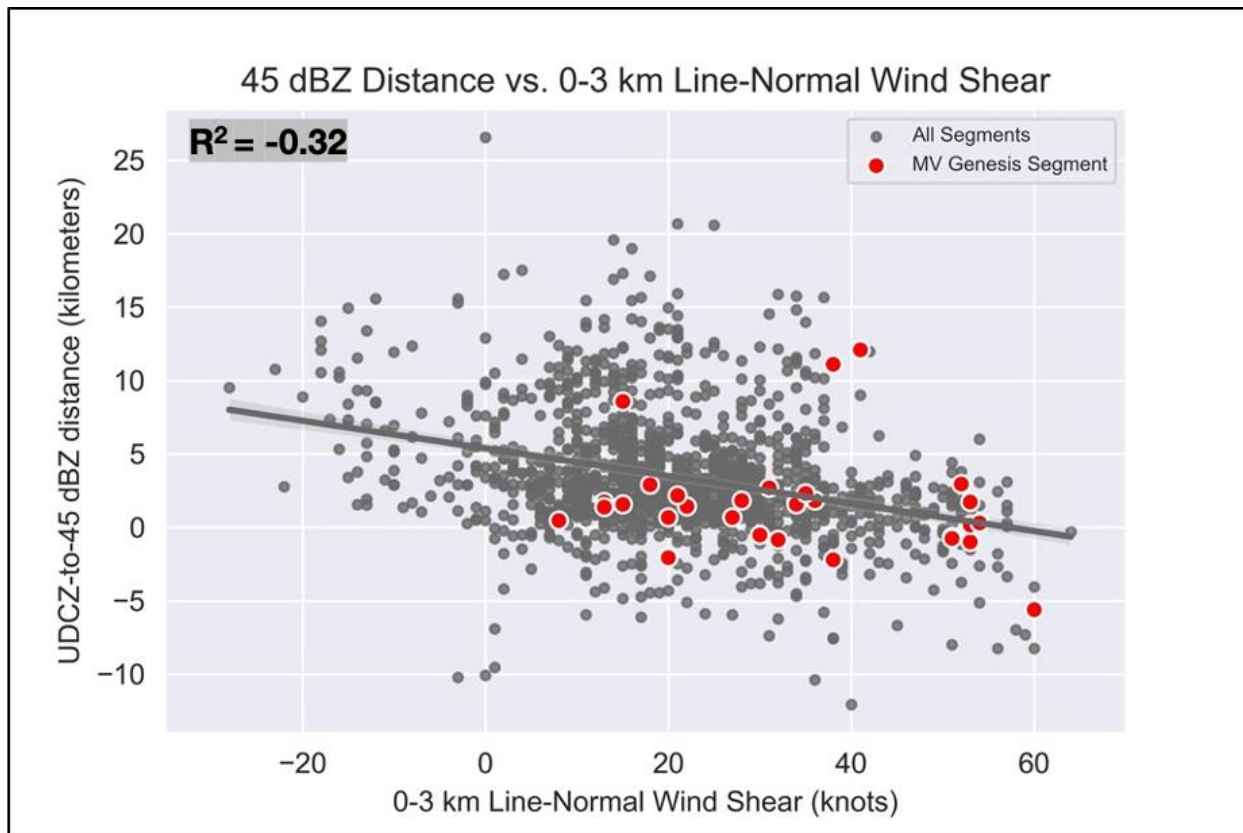
**Figure 24.** As in Fig. 23 now applying the 45 dBZ reflectivity threshold to quantify the shear/cold pool balance.
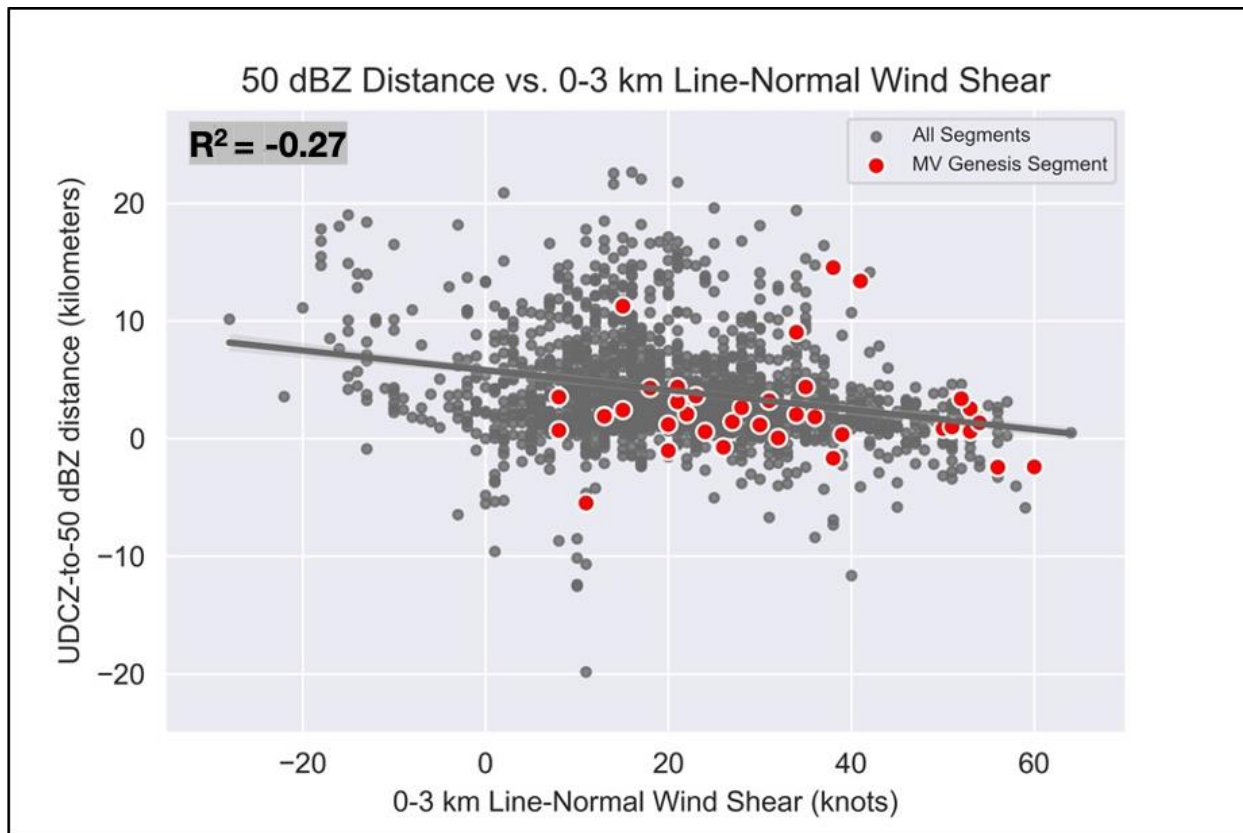
**Figure 25.** As in Fig. 23 now applying the 50 dBZ reflectivity threshold to quantify the shear/cold pool balance.
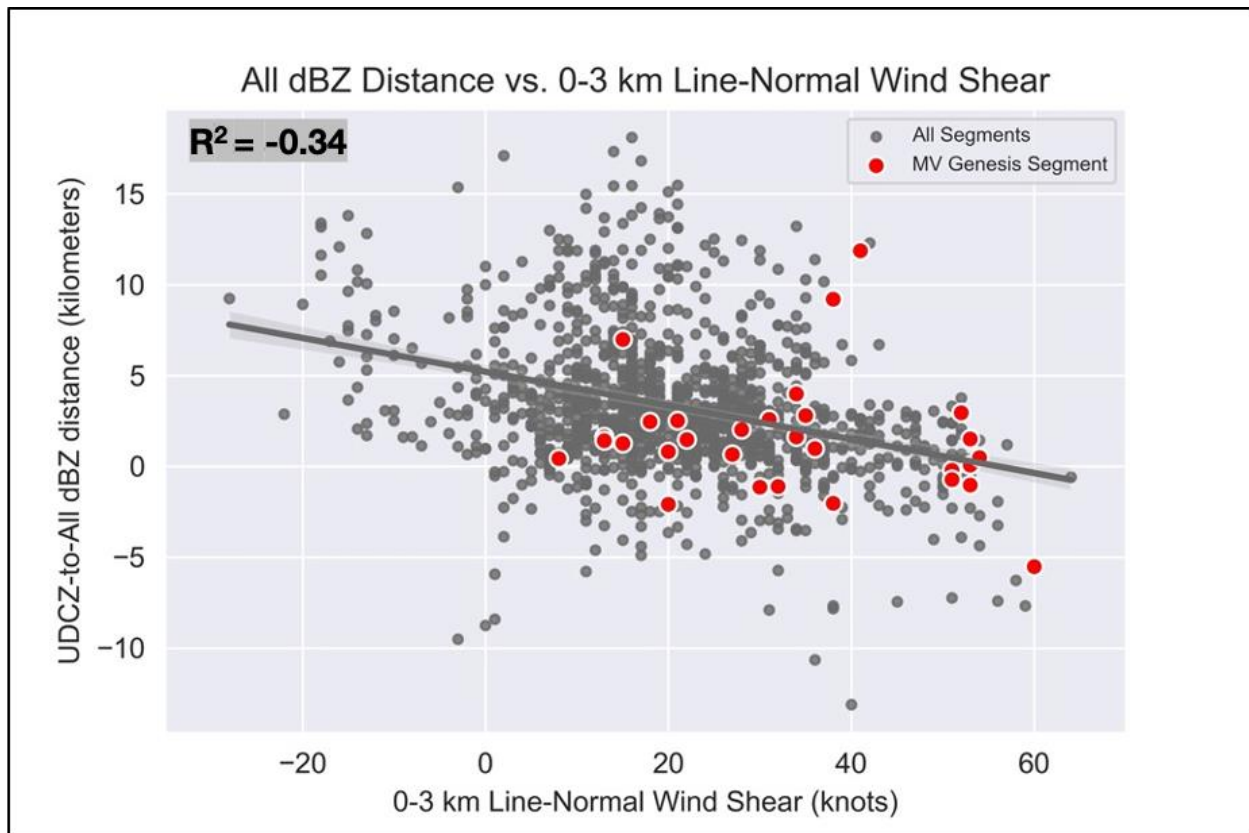
**Figure 26.** As in Fig. 23 now applying the "All" dBZ (AdBZ) reflectivity threshold to quantify the shear/cold pool balance.
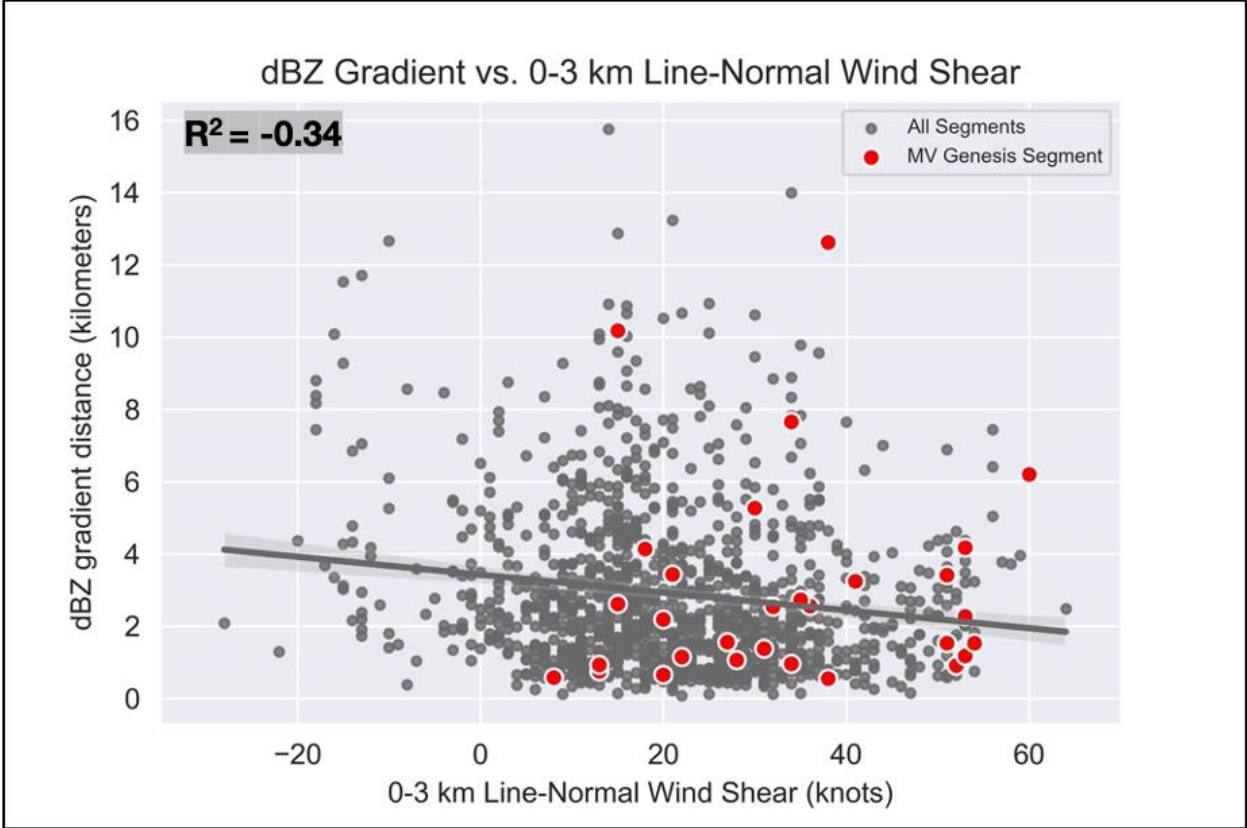
**Figure 27.** As in Fig. 23 now applying the dBZ gradient (40-to-50 dBZ distance) reflectivity threshold to quantify the shear/cold pool balance.
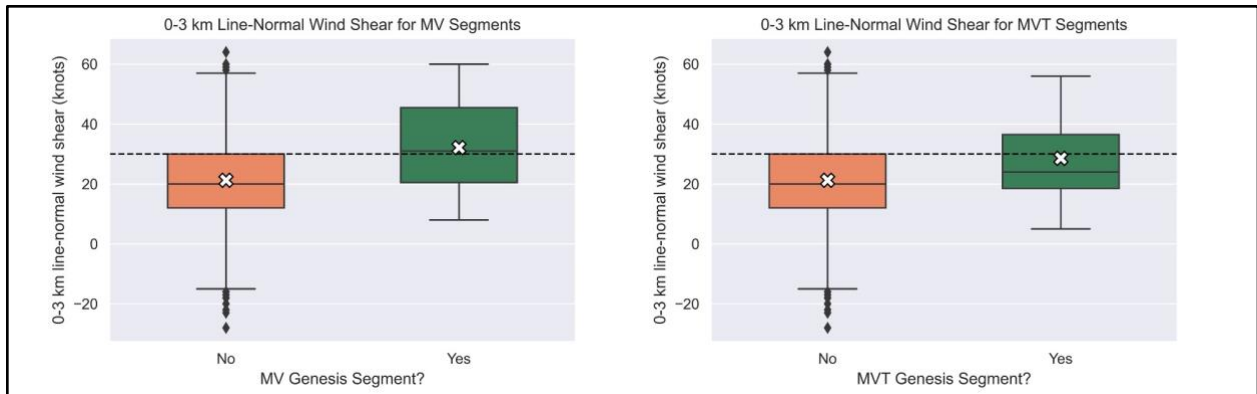
**Figure 28.** (Left panel) Boxplot of 0-3 km line-normal bulk wind shear comparing segments that observed mv-genesis versus those that did not. (Right panel) Same as the left panel now assessing segments that observed "transient" mv-genesis. Black-dashed delineates the 30 kt threshold of the 3-I-M.
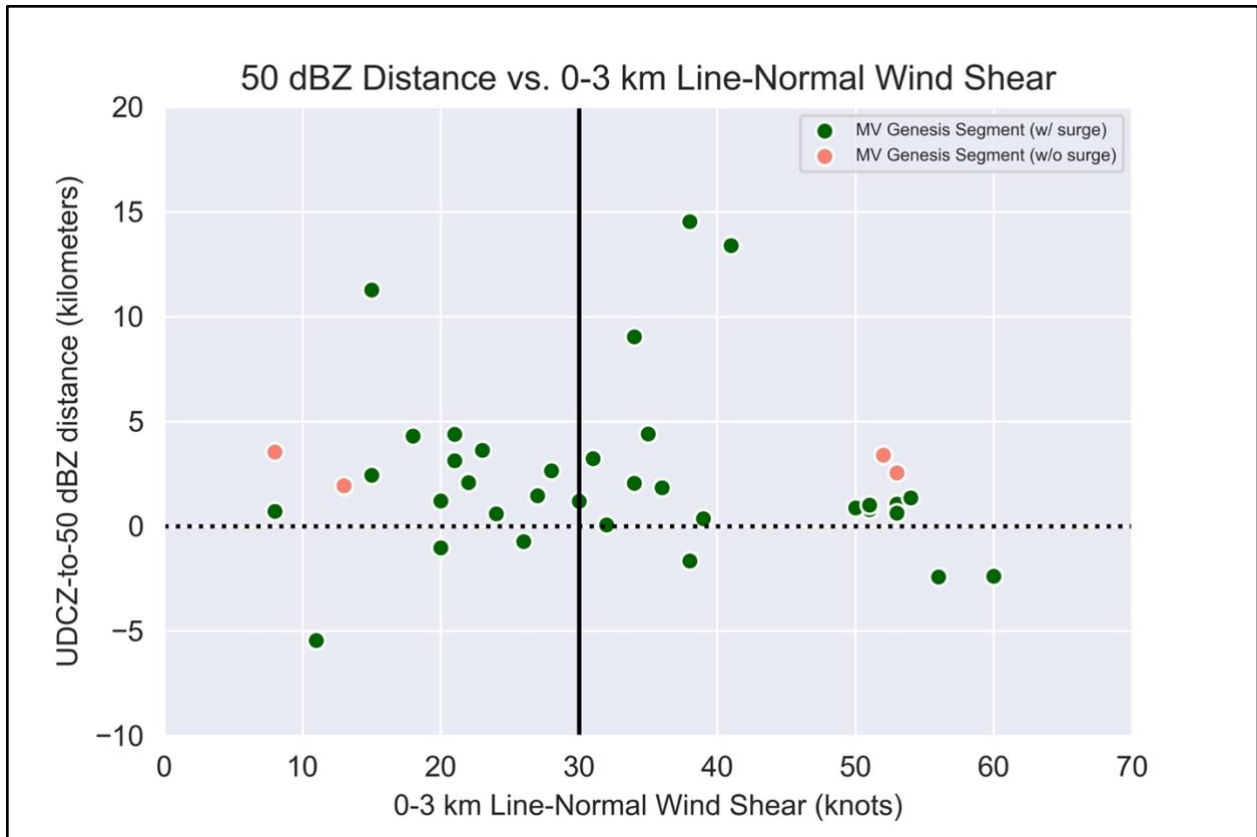
**Figure 29.** Scatterplot showing a comparison of 1st and 2nd 3-I-M ingredients, using the 50 dBZ threshold distance to quantify the shear/cold pool balance, across mv-genesis segments. Vertical black line represents the 30 kt wind shear threshold of the 3-I-M. Coloring represents subdivision based upon mv-genesis and surge occurrence.
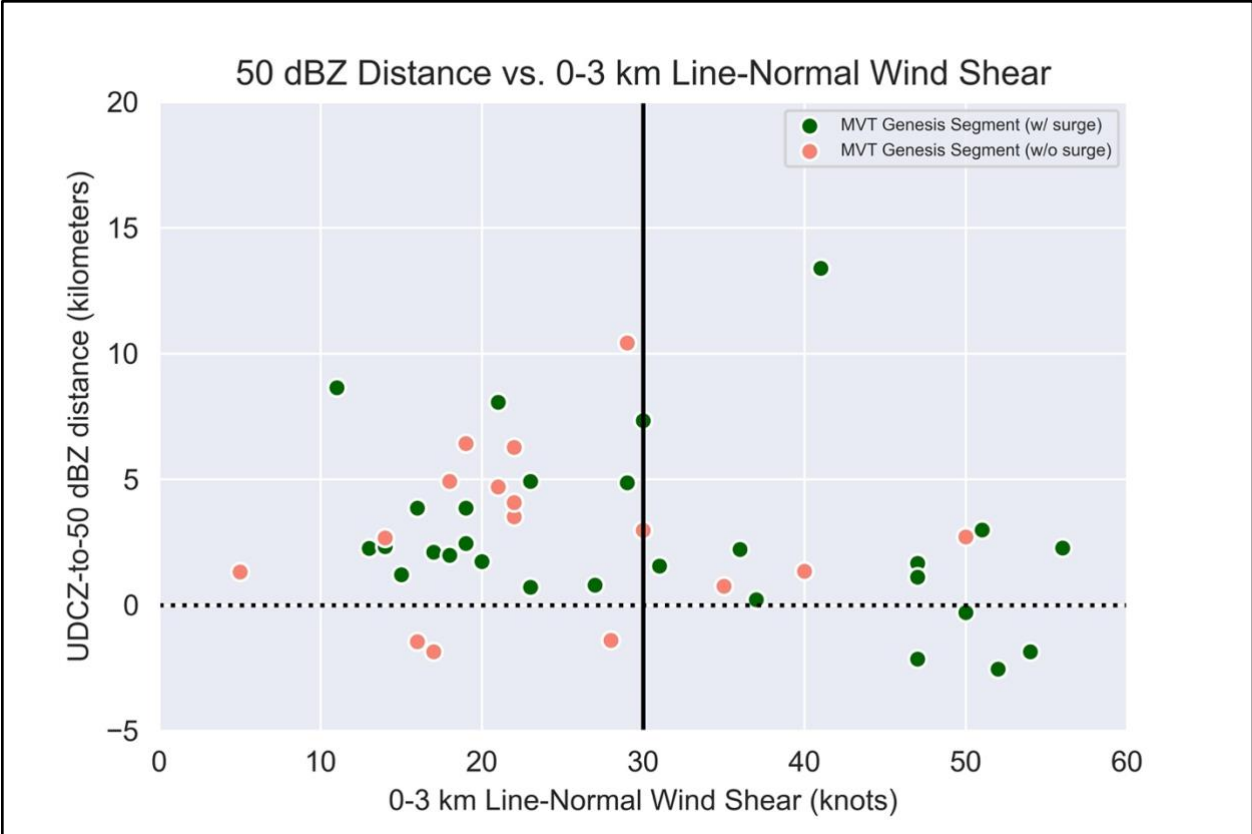
**Figure 30.** As in Fig. 29, now displaying "transient" mv-genesis.

**Figure 31.** Scatterplot comparing shear/cold balance and wind shear ingredients using the 50 dBZ reflectivity threshold and 0-1 km line-normal component. Linear regression line represented as gray line (95% confidence interval shown as light gray shading), with Pearson correlation coefficient value ($R^2$) displayed in the top left corner. Red scatters represent segments where mv-genesis was assessed.
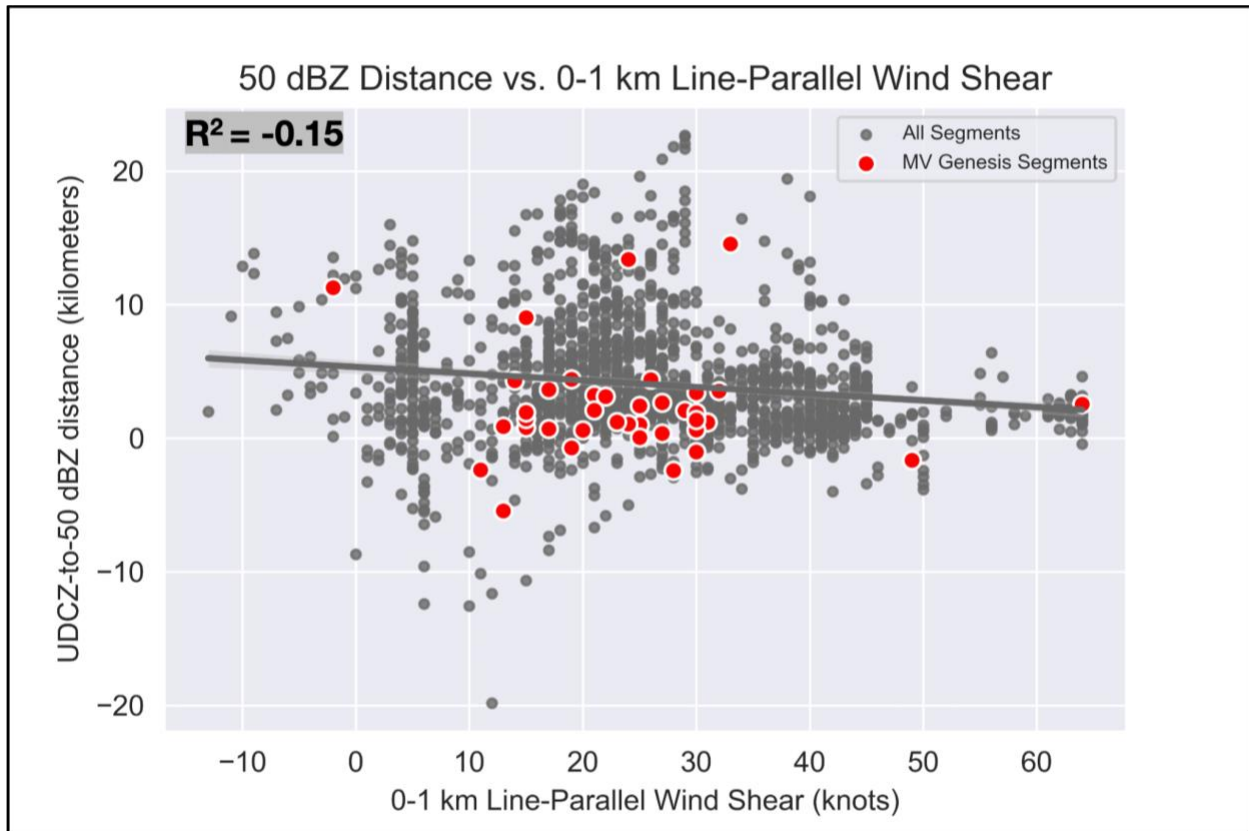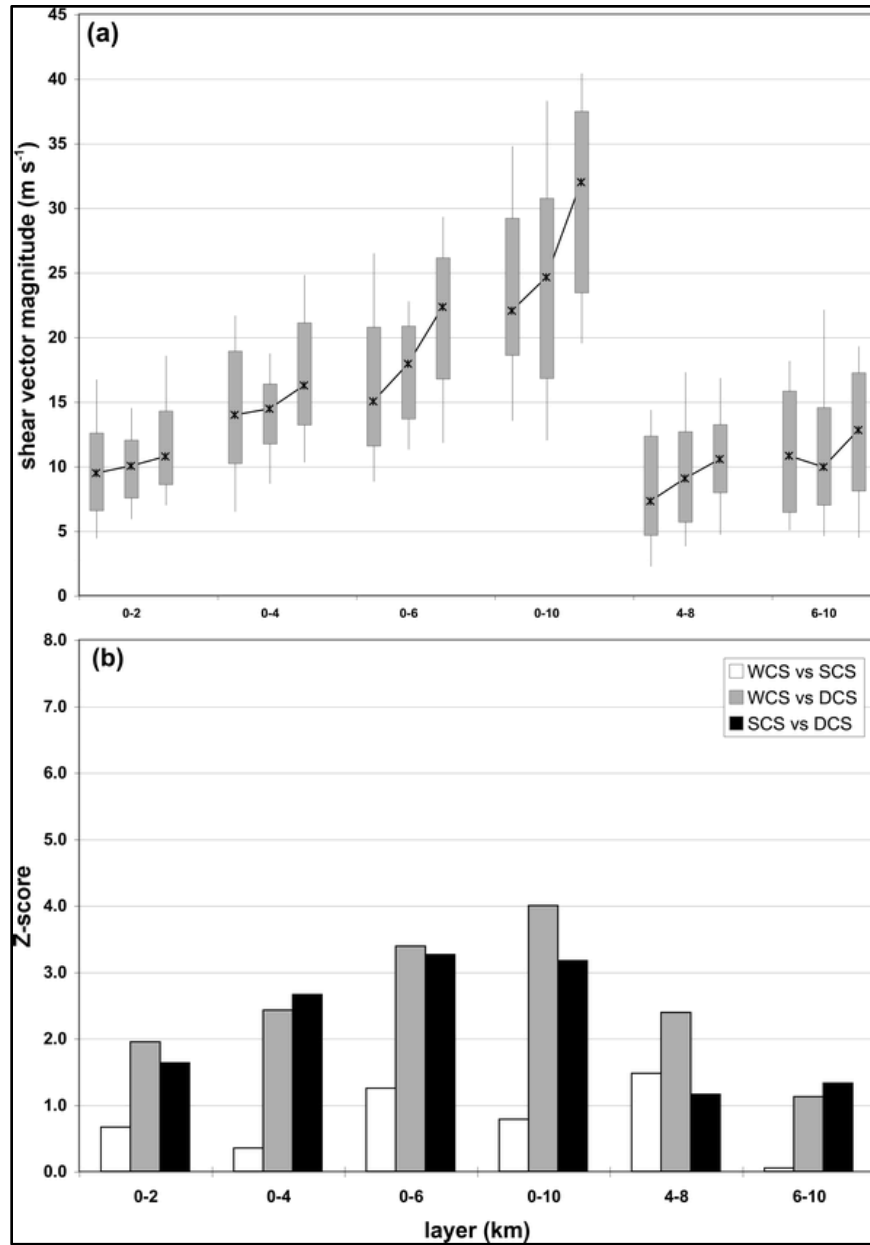
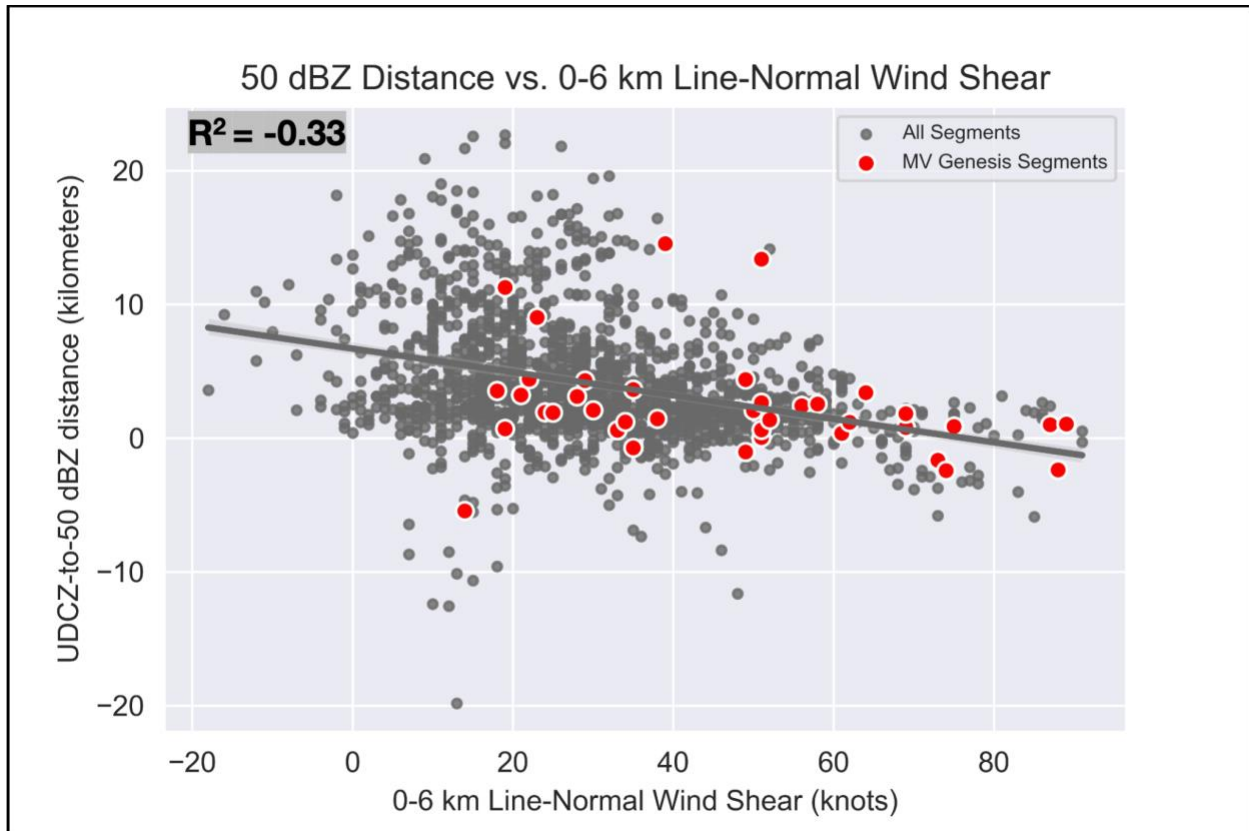**Figure 32.** Scatterplot comparing shear/cold pool balance and wind shear ingredients using the 50 dBZ reflectivity threshold and line-parallel component of 1Shear. Linear regression line represented as gray line (95% confidence interval shown as light gray shading), with Pearson correlation coefficient value ($R^2$) displayed in the top left corner. Red scatters represent segments where mv-genesis was assessed.

**Figure 33.** Breakdown of QLCS severity based upon varying magnitudes of wind shear across different atmospheric depths. Figure adapted from Cohen et al. (2007).
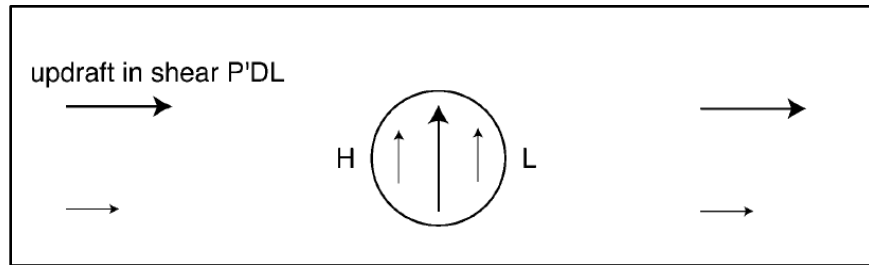
**Figure 34.** Schematic of updraft-in-shear concept. Solid arrows represent streamlines. Pressure maxima and minima represented by 'H' and 'L' respectively. Figure adapted from Parker and Johnson (2004).

**Figure 35.** Scatterplot comparing the shear/cold pool balance and wind shear 3-I-M ingredients using the 50 dBZ reflectivity threshold and in the 0-6 km line-normal wind shear component. Linear regression line represented as gray line (95% confidence interval shown as light gray shading), with Pearson correlation coefficient value ($R^2$) displayed in the top left corner. Red scatters represent segments where mv-genesis was assessed.
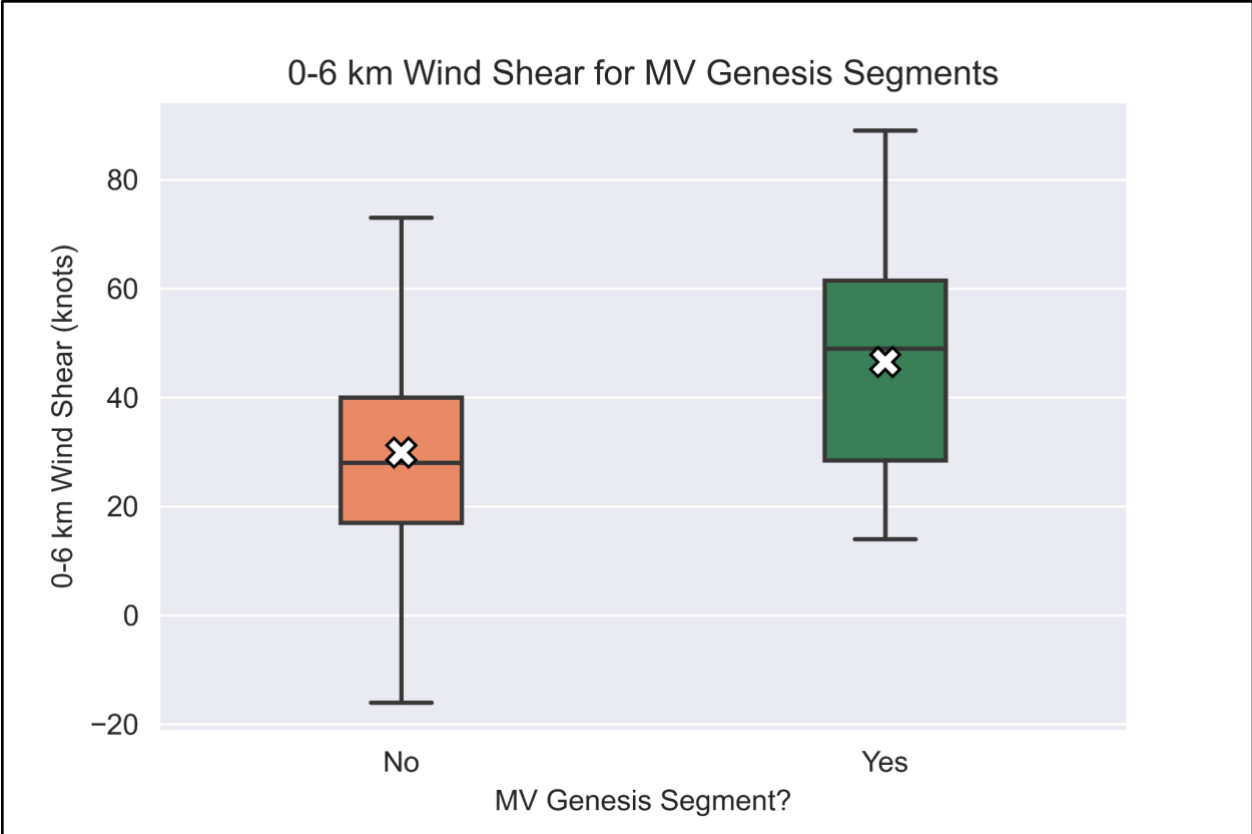
**Figure 36.** Boxplot comparison of 0-6 km line-normal bulk wind shear binned based upon mv-genesis outcome.
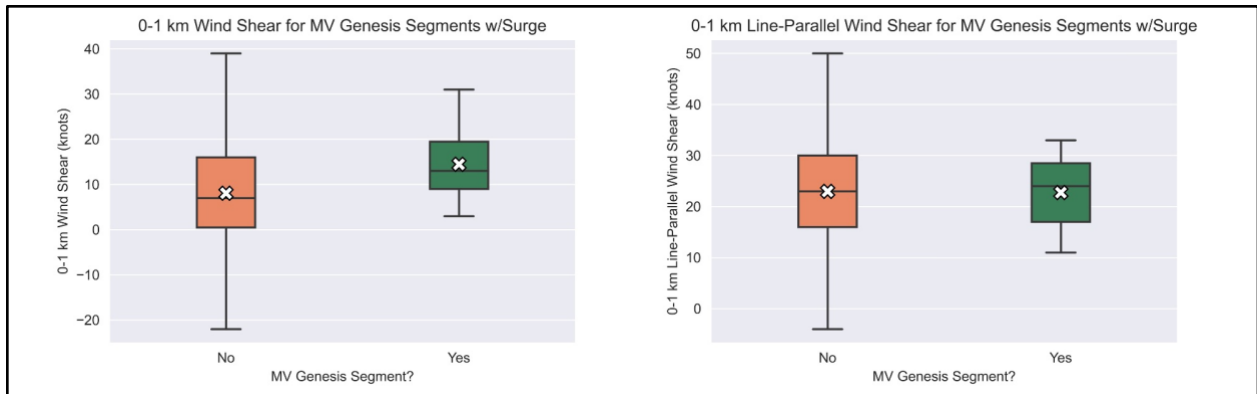
**Figure 37.** (Left panel) 0-1 km line-normal wind shear across segments observing a rear-inflow surge, subdivided based upon mv-genesis outcome. (Right panel) Same as left, now assessing 0-1 km line-parallel wind shear.
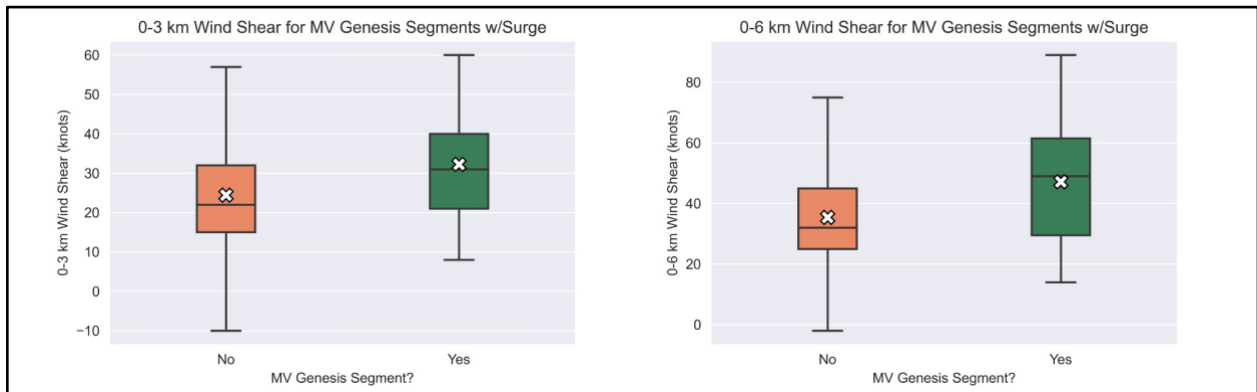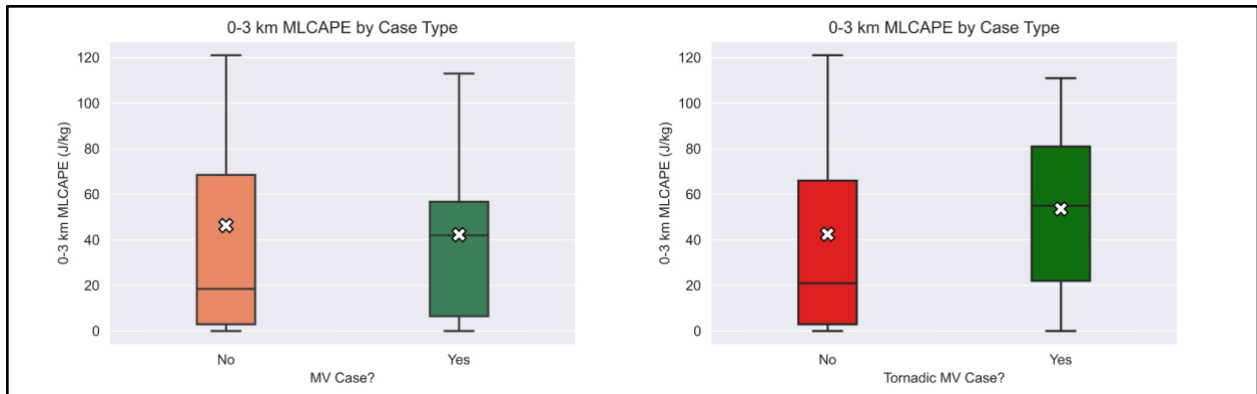


**Figure 38.** (Left panel) 0-3 km line-normal wind shear across segments observing a rear-inflow surge, subdivided based upon mv-genesis outcome. (Right panel) Same as left, now assessing 0-6 km line-normal wind shear.

**Figure 39.** Boxplot comparison of 0-3 km convective available potential energy (CAPE, J/kg) using the mixed layer parcel divided by mv-genesis (left panel) and tornadogenesis (right panel) outcomes.
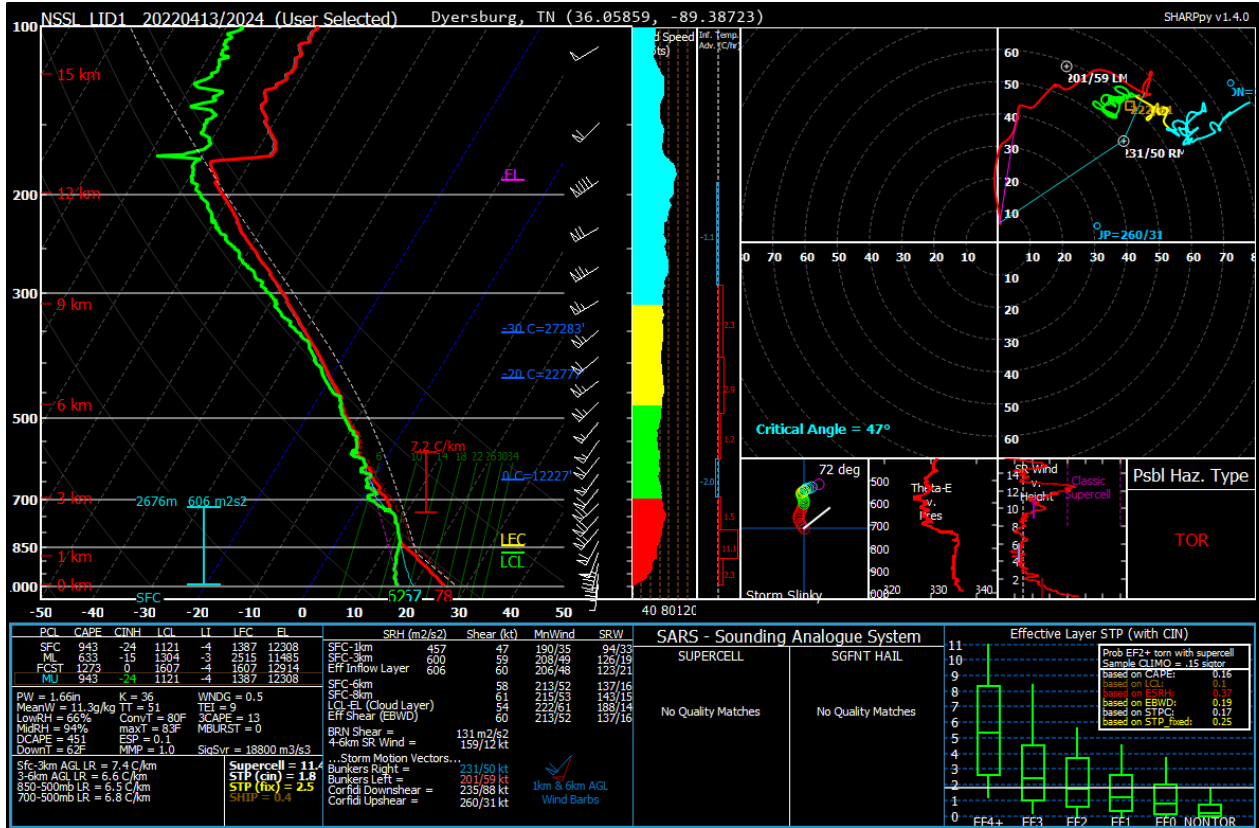
**Figure 40.** Radiosonde profile launched by National Severe Storms Laboratory Lidar team in near-proximity to an approaching QLCS. This event was associated with Intensive Operations Period #4 of the PERiLS Field Program.

**Figure 41.** Overview of National Severe Storms Laboratory Lidar truck position relative to three QLCS mesovortex tornadoes that occurred upstream across northeast Arkansas and southern Missouri. Imagery courtesy of Google Earth.
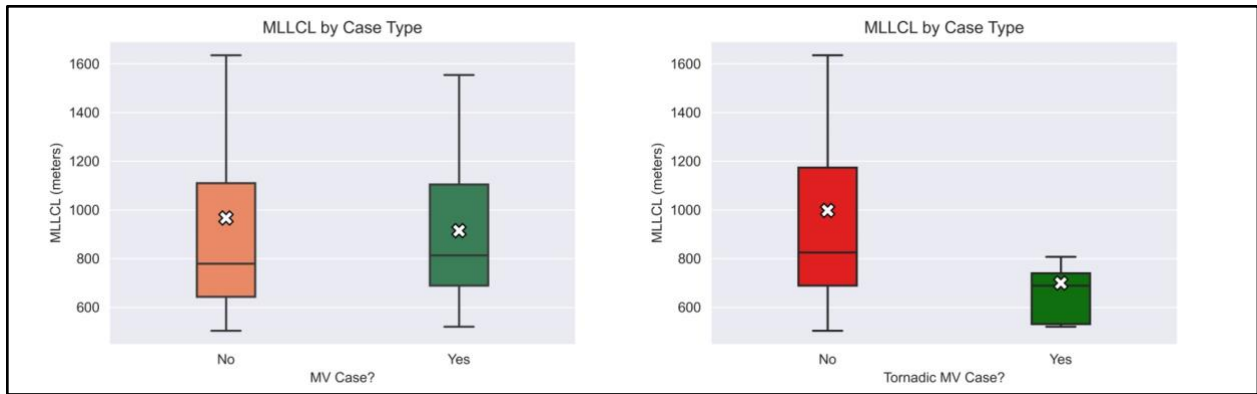
**Figure 42.** Boxplot breakdown of lifted condensation level (LCL, meters) height using mixed-layer parcel divided by mv-genesis (left panel) and tornadogenesis (right panel) outcomes.
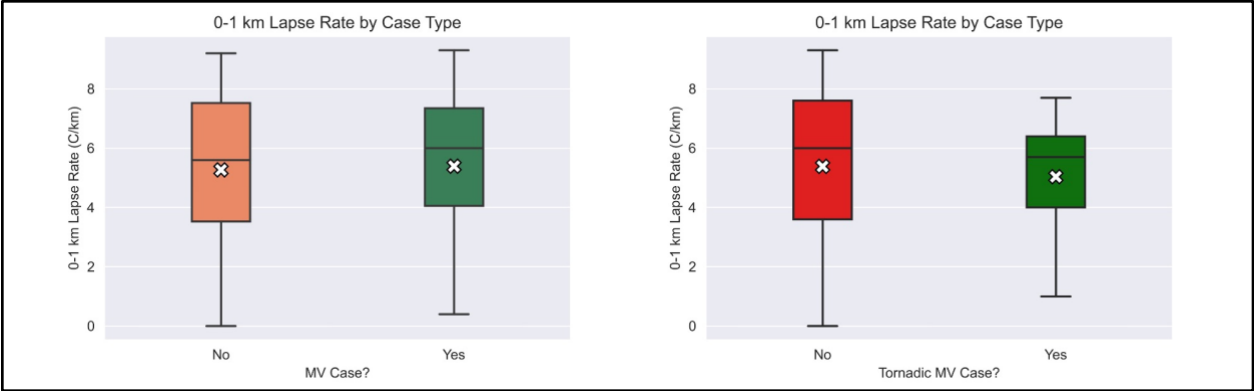
**Figure 43.** Boxplot breakdown of temperature lapse rate (C/km) in the 0-1 km depth divided by mv-genesis (left panel) and tornadogenesis (right panel) outcomes.
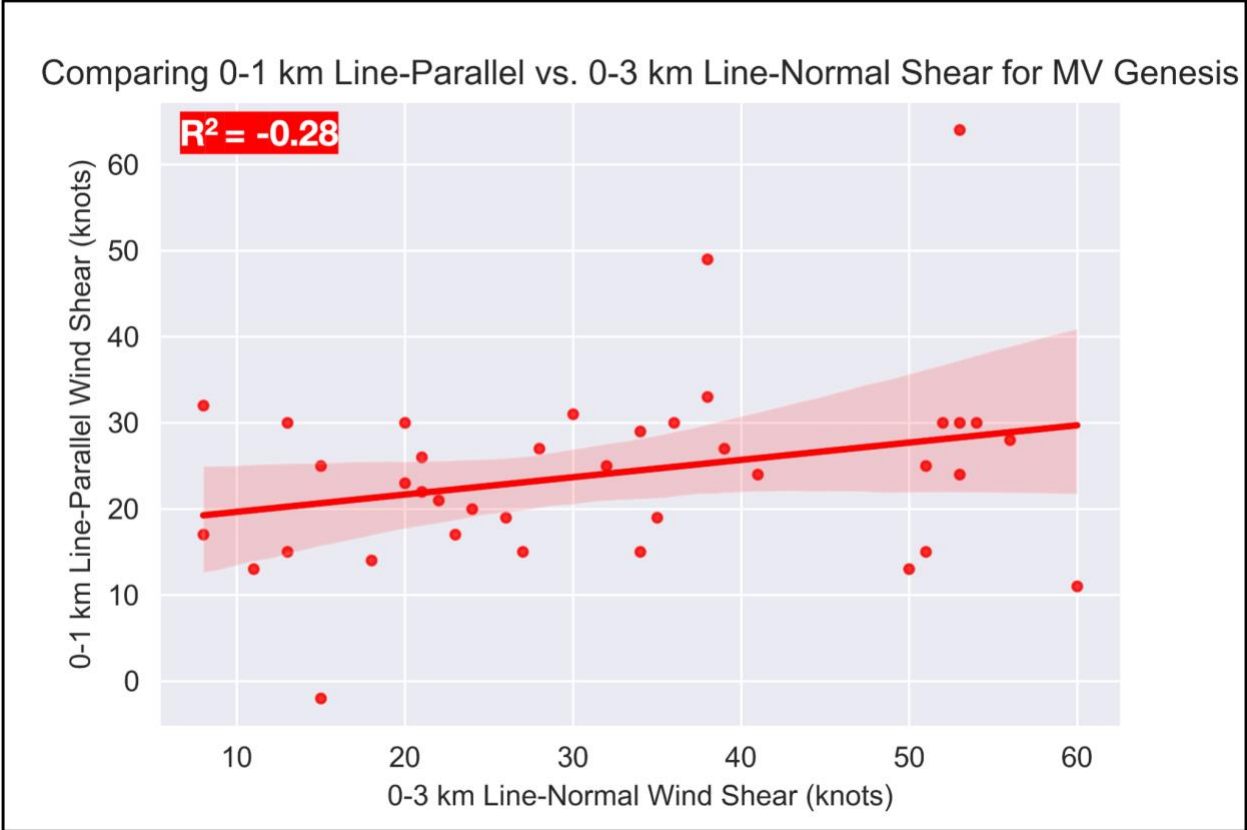
**Figure 44.** Scatterplot comparing 0-1 km line-parallel vs. 0-3 km line-normal wind shear over segments that observed mv-genesis. Linear regression line represented as red line (95% confidence interval shown as light red shading).